

General Disclaimer

One or more of the Following Statements may affect this Document

- This document has been reproduced from the best copy furnished by the organizational source. It is being released in the interest of making available as much information as possible.
- This document may contain data, which exceeds the sheet parameters. It was furnished in this condition by the organizational source and is the best copy available.
- This document may contain tone-on-tone or color graphs, charts and/or pictures, which have been reproduced in black and white.
- This document is paginated as submitted by the original source.
- Portions of this document are not fully legible due to the historical nature of some of the material. However, it is the best reproduction available from the original submission.

**NASA TECHNICAL
MEMORANDUM**

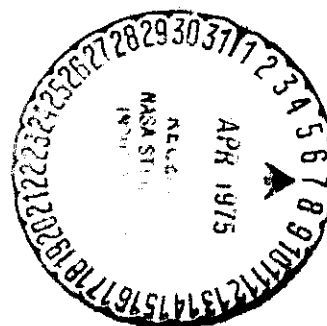
NASA TM X-71684

NASA TM X-71684

**APPLICATION OF BOUNDARY INTEGRAL EQUATIONS
TO ELASTOPLASTIC PROBLEMS**

by A. Mendelson and L. U. Albers
Lewis Research Center
Cleveland, Ohio 44135

TECHNICAL PAPER to be presented at
Applied Mechanics Conference sponsored by the
American Society of Mechanical Engineers
Troy, New York, June 23-25, 1975



(NASA-TM-X-71684) APPLICATION OF BOUNDARY
INTEGRAL EQUATIONS TO ELASTOPLASTIC PROBLEMS
(NASA) 38 p HC \$3.75 CSCL 20K

N75-19734

**Unclass
G3/39 13423**

APPLICATION OF BOUNDARY INTEGRAL EQUATIONS TO ELASTOPLASTIC PROBLEMS

A. Mendelson and L. U. Albers
NASA Lewis Research Center
Cleveland, Ohio

ABSTRACT

The application of Boundary Integral Equations to elastoplastic problems is reviewed. Details of the analysis as applied to torsion problems and to plane problems is discussed. Results are presented for the elastoplastic torsion of a square cross section bar and for the plane problem of notched beams. A comparison of different formulations as well as comparisons with experimental results are presented.

INTRODUCTION

Methods of analysis in elasticity and plasticity, as in most other scientific and engineering fields, have been revolutionized by the advent of the modern digital computer. Thus the availability of the computer made it possible to implement practically purely numerical methods such as finite difference and finite elements, as well as analytical methods such as complex variable methods.

Similarly the boundary integral equation (BIE) methods, while having their origin in classical elasticity, have only in recent years begun to play a significant role in solid mechanics. Solutions to problems in elasticity by these BIE methods have been obtained by various investigators using different formulations, as for example in Refs. (1,2). A review of much of the literature is given in Ref. (3).

The extension of the BIE method to elastoplastic problems has received much less attention. The basic theories and equations have been formulated in Refs. (3,4) but few applications have been reported. The present paper reviews some of these applications and presents details of the analyses as applied to elastoplastic torsion problems, and to the plane elastoplastic problem, with particular reference to edge-notched beams in bending. Comparisons of different formulations as well as comparisons with experimental results are presented.

ELASTOPLASTIC TORSION

The elastoplastic torsion problem can be formulated in several ways (Ref. (3)). For example, using the Prandtl stress function, F , the basic differential equation becomes

$$\nabla^2 F = -2G\alpha - 2G \left(\frac{\partial \epsilon_{zx}^p}{\partial y} - \frac{\partial \epsilon_{zy}^p}{\partial x} \right) = f(x, y) \quad (1)$$

where G is the shear modulus, α , the linear coefficient of thermal expansion and $\epsilon_{zx}^p, \epsilon_{zy}^p$ are the plastic shear strains. The corresponding BIE is

$$\pi F(p) = \iint_R f(Q) \ln r_{pQ} \, dx \, dy + \int_C \left[F'(\ln r_{pq})'_q - F' \ln r_{pq} \right] dq \quad (2)$$

where primes denote derivatives with respect to the outward normal and where the coordinate system and the associated notation are shown in Figs. 1 and 2. For an interior point P , the multiplier of $F(p)$ in Eq. (2) becomes 2π instead of π .

As an illustration of the use of Eq. (2) and its ability to solve the elastoplastic torsion problem, consider the case of a circular shaft of radius a . The radial coordinate will be designated by ρ , to distinguish it from r , the distance between the fixed point and the variable point appearing in Eq. (2). In polar coordinates, because of symmetry, the function f appearing in Eq. (2) becomes

$$f = -2G\alpha + \frac{2G}{\rho} \frac{\partial}{\partial \rho} (\rho \epsilon_{z\theta}^p) \quad (3)$$

For linear strain hardening

$$\epsilon_{z\theta}^p = A\rho + B \quad (4)$$

where

$$A = \frac{3\alpha}{2 \left[3 + 2(1+\nu) \frac{m}{1-m} \right]}$$

$$B = \frac{-\sqrt{3}(1+\nu)\epsilon_0}{3 + 2(1+\nu) \frac{m}{1-m}}$$

ν is Poisson's ratio, ϵ_0 is the yield strain, and m is the strain hardening parameter (slope of strain hardening curve divided by the modulus).

On the boundary $F(a) = 0$ and because of axial symmetry $F'(a) = \text{constant}$. Eq. (2) then becomes

$$0 = 2G \iint_R \left(2A - \alpha + \frac{B}{\rho}\right) \ln r_{pq} dx dy - F'(a) \int_C \ln r_{pq} dq \quad (5)$$

which upon solving for $F'(a)$ gives

$$F'(a) = G[2A(2A - \alpha) + 2B] \quad (6)$$

Hence for any interior point

$$2\pi F(\rho) = 2G \iint_R \left(2A - \alpha + \frac{B}{\rho}\right) \ln r_{pq} dx dy - F'(a) \int_C \ln r_{pq} dq \quad (7)$$

or

$$F(\rho) = \frac{G}{2} \left[(2A - \alpha)(\rho^2 - a^2) + 4B(\rho - a) \right] \quad (8)$$

and the shear stress τ is given by

$$\tau = -\frac{\partial F}{\partial \rho} = 2G \left[\left(\frac{\alpha}{2} - A \right) (\rho - B) \right]$$

which agrees with the solution obtained in a entirely different fashion in Ref. (5). Note that this solution is valid only in the plastic region, that is, for $\rho \leq \rho_c$, where ρ_c , the elastic plastic boundary, is given by

$$\rho_c = \frac{2(1 + \nu)\epsilon_0}{\sqrt{3}\alpha} \quad (9)$$

The formulation given by Eq. (2) can of course be used to obtain the elastoplastic solution for almost any shape cross section and any type of strain hardening. In general, however, it would seem that a formulation in terms of the warping function (axial displacement) should be preferable, since the warping function is physically more meaningful than the stress function and more importantly, the distinction between simply connected and multiply connected regions disappears. We will therefore formulate the problem in terms of the warping function and show in some detail how the solution is obtained for a bar with a square cross section.

The BIE in terms of the warping function w is (Ref. (6))

$$\pi w(p) = \iint_R f(q) \ln r_{pq} dA + \int_C w(q) (\ln r_{pq})'_q dq - \int_C w'(q) \ln r_{pq} dq \quad (10)$$

where

$$\left(\frac{\partial \epsilon_p}{\partial x} \frac{\partial p}{\partial y} + \frac{\partial \epsilon_p}{\partial y} \frac{\partial p}{\partial x} \right) \quad (11)$$

Note that Eqs. (1) and (10) imply the use of the deformation theory of plasticity. However, as shown by Prager (Ref. (7)), both the total and incremental theories of plasticity furnish the same solution to the torsion problem provided either the cross section is circular or the material is perfectly plastic. It is reasonable to assume, therefore,

that this will be approximately true for most practical problems. Indeed, it has been shown in Ref. (8) that for the case of a square cross section with strain hardening there is little difference between incremental and deformation theories. The use of incremental theory does not appreciably complicate the problem and can be used in a stepwise manner as for the plane problems to be discussed subsequently.

The boundary condition to be satisfied by the warping function is (Ref. (6))

$$\frac{\partial w}{\partial n} = w' = \alpha(\ell y - m x) + 2\left(\ell \epsilon_{xz}^p + m \epsilon_{yz}^p\right) \quad (12)$$

where ℓ, m are the direction cosines of the outward normal, and where for a rectangular boundary segment parallel to one of the coordinate axes, the second term on the right side of Eq. (12) always vanishes. The normal derivative of the warping function appearing in Eq. (10) is thus known from Eq. (12) and the only unknown in Eq. (10) is $w(p)$.

Numerical Procedure

To solve Eq. (10) for the unknown function $w(p)$, the straightforward procedure of replacing the integrals by summations can be used. The boundary is divided into n intervals with a nodal point taken at the center of each interval. The unknown function is assumed constant over each interval. Similarly, the region R is divided into a number of cells and the function f assumed constant over each cell. Eq. (10) is then written for each nodal point as follows:

$$\sum_{j=1}^n (a_{ij} - \delta_{ij}\pi) w_j = \sum_{j=1}^n b_{ij} w_j + R_i \quad i = 1, 2, \dots, n \quad (13)$$

The coefficients a_{ij} , b_{ij} , and R_i are given in Appendix A. We thus have n equations for the n unknowns, w_j . This set of equations can readily be solved by any standard procedure.

Once the w_j are known on the boundary, Eq. (10) can be used to calculate w at any interior point, with π replaced by 2π . However, in order to calculate the strains the derivatives of w are needed. These can be obtained by differentiating Eq. (10) under the integral sign to give

$$\begin{aligned} \frac{\partial w(P)}{\partial x} = & \frac{1}{2\pi} \iint_R f(Q) \frac{x_P - x_Q}{r_{PQ}^2} dx dy \\ & + \frac{1}{2\pi} \int_C w(Q) \frac{[(x_P - x_Q)^2 - (y_P - y_Q)^2] \ell_Q + 2(x_P - x_Q)(y_P - y_Q) m_Q}{r_{PQ}^4} dq \\ & - \frac{1}{2\pi} \int_C w'(Q) \frac{x_P - x_Q}{r_{PQ}^2} dq \end{aligned} \quad (14)$$

For $\partial w(P)/\partial y$ we interchange x and y .

Again the integrals are replaced by sums resulting in

$$\frac{\partial w(x_i, y_j)}{\partial x} = \frac{1}{2\pi} \left[\sum_{k=1}^n (w_k^l A_{ijk} + w_k^m B_{ijk} - w_k^l C_{ijk}) + \sum_{k,l} f_{kl} D_{ijkl} \right] \quad (15)$$

where the coefficients A_{ijk} , B_{ijk} , C_{ijk} , and D_{ijkl} are listed in Appendix A. $\sum_{k,l}$ is the sum for all the plastic cells in the region.

From the derivatives of w the total strains are computed as

$$\left. \begin{aligned} \epsilon_{xz} &= \frac{1}{2} \left(\alpha y + \frac{\partial w}{\partial x} \right) \\ \epsilon_{yz} &= \frac{1}{2} \left(\alpha x + \frac{\partial w}{\partial y} \right) \end{aligned} \right\} \quad (16)$$

The plastic strains appearing in the definition of the function $f(x, y)$ are of course in turn nonlinear functions of the warping function w . They can be determined from

$$\left. \begin{aligned} \epsilon_{xz}^p &= \frac{\epsilon_p}{\epsilon_{et}} \epsilon_{xz} \\ \epsilon_{yz}^p &= \frac{\epsilon_p}{\epsilon_{et}} \epsilon_{yz} \end{aligned} \right\} \quad (17)$$

where

$$\epsilon_{et} = \frac{2}{\sqrt{3}} \sqrt{(\epsilon_{xz})^2 + (\epsilon_{yz})^2} \quad (18)$$

and

$$\epsilon_p = f(\epsilon_{et}) \quad (19)$$

Eq. (19) represents the uniaxial stress-strain curve in terms of equivalent plastic strain against equivalent total strain; that is,

$$\epsilon_p = \epsilon_{et} - \frac{1}{3} \frac{\sigma_e}{G} \quad (20)$$

where σ_e , the equivalent stress, represents the stress on the uniaxial stress-strain curve and ϵ_p the plastic strain on that curve. Thus, for a given stress-strain curve, the relation between ϵ_p and ϵ_{et} represented by Eq. (19) can be determined using Eq. (20). For the case of linear strain hardening, the relation (19) can be written as

$$\epsilon_p = \frac{\epsilon_{et} - \frac{2}{3} (1 + \nu) \epsilon_0}{1 + \frac{2}{3} (1 + \nu) \frac{m}{1 - m}} \quad (21)$$

Since as noted the function f is implicitly a nonlinear function of the warping function w , the solution is obtained iteratively by starting with $f = 0$ and calculating improved values via Eqs. (13), (15), (16), (17), (11), and back to (13), etc. This is the method of successive elastic solutions or method of initial strains. The tangent modulus method could be used equally well and may save on computer time. Complete details of the calculations performed herein are given in Ref. (6).

Results

Calculations were performed by this technique for a bar of square cross section as shown in Fig. 3. The dimensionless angle of twist per unit length β , defined as $\alpha a/\epsilon_0$, where a is $1/2$ the side of the square, was increased in steps of one from $\beta = 1$ to $\beta = 6$. Linear strain hardening was assumed with values of the strain hardening parameter taken as 0 (perfect plasticity), 0.05, 0.1, and 0.2. Poisson's ratio was assumed as 0.3 in all calculations.

For $\beta = 1$, the bar is elastic and a comparison was made between the analytical solution as given, for example, in Ref. (9) as well as with the finite difference solution of Ref. (10). The results are shown in Tables I to III. Table I shows the warping function as computed on the boundary of the bar cross section. The comparison with the analytical solution of Ref. (9) shows very good agreement with just four unknowns to solve for in the boundary integral method.

Table II shows the comparison for the maximum shear stress (at the center of the edge of the square) and the moment with the analytical solution of Ref. (9) and the finite difference solution of Ref. (10). Again it is seen that with just four unknowns in the boundary integral method very good results are obtained, as good as the results obtained for the finite difference method using 55 unknowns.

Table III presents the dimensionless shear stress distribution in the x -direction ($\tau_{xz}/2G\epsilon_0$) throughout the cross section using 10 unknowns for the boundary integral method and 55 unknowns for the finite difference method. Again excellent agreement was obtained. Actually, the results with four unknowns using the boundary integral method are almost as good, but the results with 10 unknowns are presented to match the actual (x, y) values of the finite difference results without having to cross plot.

The dimensionless angle of twist per unit length β was then increased in unit steps to a maximum value of $\beta = 6$ for each value of the strain hardening parameter m . The total boundary was divided into 80 intervals resulting in 10 equations for 10 unknowns. Several test calculations were made with fewer intervals, and the results indicated that using 48 intervals (six unknowns) changed the moment and maximum stress by at most one in the third significant figure and changed the maximum plastic strain by about 3 percent. All the subsequent results are therefore shown for 80 intervals (10 unknowns), although from an engineering viewpoint 48 or even 32 intervals would be sufficient.

The results of the calculations are summarized in Table IV and Figs. 4 to 6. Fig. 4 shows the dimensionless moment defined as $M^* = M/2G\epsilon_0 a^3$ for various values of β and m . Fig. 5 shows the corresponding dimensionless maximum shear stresses defined as $\tau_{\max} = \tau/2G\epsilon_0$ and Fig. 6 shows the spread of the plastic zones with an increase of the angle of twist β .

The degree of convergence of the iterative process was determined from a relation of the form

$$\frac{1}{M} \sum_{i=1}^M \left| \epsilon_x^p(P_i)_k - \epsilon_x^p(P_i)_{k-1} \right| < K \quad (22)$$

where M is the total number of points P_i flowing plastically and $k-1$ and k are two successive iterations. The convergence criterion K can be made as small as desired. In all the calculations the convergence number K was taken either as 0.0001 or 0.00001. In many of the calculations both numbers were used in turn. The differences in the results were found to be insignificant. For example, the number of iterations for convergence for the case of maximum plastic flow, which occurred for $\beta = 6$ and $m = 0$, was 39 for $K = 0.0001$ and 53 for $K = 0.00001$, and the results were all the same to at least three significant figures. For the case $\beta = 5$ and $M = 0$, the number of iterations for $K = 0.0001$ was 33. For the same case using finite differences, 203 iterations were required.

The boundary integral method is thus seen to be very suitable for the elastoplastic analysis of the torsion of prismatic bars. Very good accuracy can be obtained by using relatively small sets of linear algebraic equations.

A comparison with the finite difference method indicates a great savings in the number of unknowns that have to be determined and also a much faster convergence rate using the method of successive elastic solutions for both formulations. This should be reflected in appreciable savings in computer time, although computer time is not a limiting factor in any case for the torsion problem.

The boundary integral method can readily be programmed in a straightforward manner for a digital computer. The use of the warping function to formulate the problem permits applying the method with equal ease to both simply connected and multiply connected bodies.

THE PLANE PROBLEM

As for the torsion problem, the plane problem can be formulated in several ways, as a nonhomogeneous biharmonic problem for the stress function (Ref. (3)), or in terms of the Navier equations of equilibrium for the displacements (Refs. 3, 4). Both methods will be applied herein to the problem of an edge-notched beam in pure bending.

The Biharmonic Formulation

The problem of determining the state of stress and strain in a plane elastoplastic problem can be reduced to solving the following inhomogeneous biharmonic equation for the Airy stress function, ϕ , as shown in Ref. (5)

$$\nabla^4 \phi = g(x, y) \quad (23)$$

$$g(x, y) = -\frac{E}{1-\mu^2} \left[\frac{1}{y^2} \left(\epsilon_x^p + \Delta \epsilon_x^p \right) + \frac{1}{x^2} \left(\epsilon_y^p + \Delta \epsilon_y^p \right) - 2 \frac{1}{xy} \left(\epsilon_{xy}^p + \Delta \epsilon_{xy}^p \right) \right] + \frac{\mu E}{1-\mu^2} \nabla^2 \left(\epsilon_x^p + \Delta \epsilon_x^p + \epsilon_y^p + \Delta \epsilon_y^p \right) \quad (24)$$

for the plane strain case, and

$$g(x, y) = -E \left[\frac{\partial^2}{\partial y^2} (\epsilon_x^p + \Delta \epsilon_x^p) + \frac{\partial^2}{\partial x^2} (\epsilon_y^p + \Delta \epsilon_y^p) - 2 \frac{\partial^2}{\partial x \partial y} (\epsilon_{xy}^p + \Delta \epsilon_{xy}^p) \right] \quad (25)$$

for the plane stress case, where ϵ_x^p , ϵ_y^p , and ϵ_{xy}^p represent the accumulation of plastic strain increments from the beginning of the loading history up to, but not including the current increment of the load, and $\Delta \epsilon_x^p$, $\Delta \epsilon_y^p$, and $\Delta \epsilon_{xy}^p$ are the increments of plastic strain due to the current increment of load.

The stress function φ must satisfy appropriate boundary conditions. For the problem under consideration (Fig. 7), $\varphi(x, y)$ and its outward normal derivative $\partial \varphi / \partial n$ must satisfy the following boundary conditions (Ref. (11)):

$$\left. \begin{aligned} \varphi(x, y) = 0; \quad \frac{\partial \varphi}{\partial n} = 0 & \quad \text{along boundary OA and OA'} \\ \varphi(x, y) = 0; \quad \frac{\partial \varphi}{\partial n} = 0 & \quad \text{along boundary AB and A'B'} \\ \varphi(x, y) = -\frac{\sigma_{\max}}{w} \left(\frac{x^3}{3} + ax^2 + a^2x + \frac{a^3}{3} \right) + \sigma_{\max} \left(\frac{x^2}{2} + ax + \frac{a^2}{2} \right); \\ \frac{\partial \varphi}{\partial n} = 0 & \quad \text{along boundary BC and B'C'} \\ \varphi(x, y) = \frac{\sigma_{\max} w^2}{6}; \quad \frac{\partial \varphi}{\partial n} = 0 & \quad \text{along boundary CD and C'D'} \end{aligned} \right\} \quad (26)$$

To solve Eq. (23) by means of the boundary integral method, use is made of Green's second theorem to reduce this equation to coupled integral equations, as shown in Refs. (3) and (11). The result is

$$8\pi\varphi(x, y) - \iint_R \rho g(\xi, \eta) d\xi d\eta = \int_C \left[\varphi \frac{\partial}{\partial n} (\nabla^2 \rho) - \frac{\partial \varphi}{\partial n} \nabla^2 \rho + \varphi \frac{\partial \rho}{\partial n} - \frac{\partial \varphi}{\partial n} \rho \right] dq \quad \text{for } P \in R \quad (27)$$

$$4\pi\varphi(x, y) - \iint_R \rho g(\xi, \eta) d\xi d\eta = \int_C \left[\varphi \frac{\partial}{\partial n} (\nabla^2 \rho) - \frac{\partial \varphi}{\partial n} \nabla^2 \rho + \varphi \frac{\partial \rho}{\partial n} - \frac{\partial \varphi}{\partial n} \rho \right] dq \quad \text{for } P \in C \quad (28)$$

and

$$2\pi\varphi(x, y) - \iint_R g(\xi, \eta) \ln r d\xi d\eta = \int_C \left[\varphi \frac{\partial}{\partial n} (\ln r) - \frac{\partial \varphi}{\partial n} \ln r \right] dq \quad \text{for } P \in R \quad (29)$$

$$\pi\Phi(x, y) - \iint_R g(\xi, \eta) \ln r \, d\xi \, d\eta = \int_C \left[\Phi \frac{\partial}{\partial n} (\ln r) - \frac{\partial \Phi}{\partial n} \ln r \right] dq \quad \text{for } P \in C \quad (30)$$

where

$$\Phi = \nabla^2 \varphi$$

$$\rho = r^2 \ln r$$

and $r(x, y; \xi, \eta)$ is the distance between any two points $P(x, y)$ and $q(\xi, \eta)$ in the region R bounded by the curve C , such that $P \in R + C$ and $q \in C$ (Fig. 8).

Eq. (27) would, for a known function $g(x, y)$, give us directly a solution to the biharmonic Eq. (23) provided the functions $\varphi(x, y)$, $\partial\varphi(x, y)/\partial n$, $\nabla^2\varphi(x, y)$, and $\partial[\nabla^2\varphi(x, y)]/\partial n$ were known on the boundary C .

However, only the stress function φ and its outward normal derivative $\partial\varphi/\partial n$ are specified (Eq. (26)). The values of $\nabla^2\varphi = \Phi$ and $\partial(\nabla^2\varphi)/\partial n = \partial\Phi/\partial n$ on the boundary must be compatible with the given values of φ and $\partial\varphi/\partial n$. To assure this compatibility, we have to solve the system of coupled integral Eqs. (28) and (30), which contain the unknown functions Φ and $\partial\Phi/\partial n$.

Once the values of Φ and $\partial\Phi/\partial n$ on the boundary C of region R are known we can proceed with the calculation of the stress field in the region R utilizing Eq. (27) and the equations which define φ , namely,

$$\sigma_x = \frac{\partial^2 \varphi}{\partial y^2}, \quad \sigma_y = \frac{\partial^2 \varphi}{\partial x^2}, \quad \tau_{xy} = -\frac{\partial^2 \varphi}{\partial x \partial y} \quad (31)$$

The calculation of the function $g(x, y)$, which is obtained iteratively, will be discussed subsequently.

Solution of the Integral Equations

To solve the system of coupled integral equations analytically, a numerical method is utilized in which the integral Eqs. (28) and (30) are replaced by a system of simultaneous algebraic equations.

For simplicity of notation the normal derivatives are denoted by prime superscripts. The boundary is divided into n intervals, not necessarily equal, numbered consecutively in the direction of increasing q . The center of each interval is designated as a node. The values of Φ and Φ' are assumed constant on each interval and equal to the values calculated at the node.

In similar manner the interior of region R is covered by a grid, containing m cells. The cells do not have to have equal areas. Their nodal points are located at the centroids. The value of $g(\xi, \eta)$ is assumed constant over each cell and equal to the value calculated at the centroid. The arrangement of boundary and interior subdivisions is shown in Figs. 9 and 10.

Using these assumptions, Eqs. (28) and (30) can be replaced by a system of $2n$ simultaneous algebraic equations with $2n$ unknowns, that is, Φ_i and Φ'_i .

$$\left. \begin{aligned} \pi\phi_i - \sum_{k=1}^m \ln r_{ik} (gA)_k &= \sum_{j=1}^n (a_{ij}\phi_j + b_{ij}\phi_j') \\ 4\pi\phi_i - \sum_{k=1}^m \rho_{ik} (gA)_k &= \sum_{j=1}^n (c_{ij}\phi_j + d_{ij}\phi_j' + e_{ij}\phi_j'' + f_{ij}\phi_j''') \end{aligned} \right\} \quad (32)$$

where $i = 1, 2, 3, \dots, n$, r_{ik} is the distance from i^{th} node to the centroid of the k^{th} cell, A_k is the area of the k^{th} cell, and

$$\left. \begin{aligned} a_{ij} &= \int_j (\ln r_{ij})' dq \\ b_{ij} &= - \int_j \ln r_{ij} dq \\ c_{ij} &= \int_j \rho_{ij} dq \\ d_{ij} &= - \int_j \rho_{ij} dq \\ e_{ij} &= \int_j (\nabla^2 \rho_{ij})' dq \\ f_{ij} &= - \int_j \nabla^2 \rho_{ij} dq \end{aligned} \right\} \quad (33)$$

where integration is taken over the j^{th} interval, and r_{ij} is the distance from i^{th} node to any point in the j^{th} interval. The normal derivatives in Eqs. (33) are taken on the j^{th} interval.

For curved boundaries the coefficients given by Eqs. (33) can be evaluated, if necessary, by Simpson's rule for $i \neq j$. For $i = j$, because of the singular nature of the integrand, the integrals for the coefficients must be evaluated by a limiting process. For boundary intervals, such as for the problem treated herein, which can be represented by straight lines a closed form solution can be obtained for these coefficients.

Boundary Eqs. (32) expressed in matrix form become

$$\left\{ \begin{bmatrix} [a_{ij} - \delta_{ij}\pi] & [b_{ij}] \\ [c_{ij}] & [d_{ij}] \end{bmatrix} \begin{bmatrix} [\phi_j] \\ [\phi_j'] \end{bmatrix} \right\} = - \left\{ \begin{bmatrix} [\ln r_{ik}] & [0] & [0] \\ [\rho_{ik}] & [e_{ij} - \delta_{ij}4\pi] & [f_{ij}] \end{bmatrix} \begin{bmatrix} [(gA)_k] \\ [\phi_j] \\ [\phi_j'] \end{bmatrix} \right\} \quad (34)$$

Thus, the problem is reduced to the solution of the following matrix system:

$$[B]\{X\} = \{R\} \quad (35)$$

where $[B]$ is $2n \times 2n$ matrix and $\{X\}$ and $\{R\}$ are $2n \times 1$ column matrices.

Matrix $[B]$ is dependent only on geometry, that is, number of nodes and their distribution on the boundary. Since the matrix $\{R\}$ contains the nonlinear function $g(\xi, \eta)$, which depends on the stress field and therefore on matrix $\{X\}$, an iterative process will be used to obtain the solution.

To calculate stresses, at any nodal point in the region R , from the stress function ϕ , we need not perform any numerical differentiation. Eq. (27) can be differentiated under the integral sign and once ϕ and ϕ' are known on the boundary the stresses can be obtained by the same type of numerical integration as in Eqs. (32). Applying Eqs. (31) to Eq. (27) yields for the case of a rectangular grid the following stress equations:

$$\left. \begin{aligned} 8\pi\sigma_x(x, y)_i &= \left\{ \left[\ln \left(\frac{\delta_x^2 + \delta_y^2}{4} \right) + \frac{2\delta_y}{\delta_x} \tan^{-1} \frac{\delta_x}{\delta_y} - 1 \right] (gA)_k + \sum_{k=1}^m \left\{ \ln [(x-\xi)^2 + (y-\eta)^2] \right. \right. \\ &\quad \left. \left. + \frac{2(y-\eta)^2}{(x-\xi)^2 + (y-\eta)^2} + 1 \right\} (gA)_k + \sum_{j=1}^n (A_{ij}\phi_j + B_{ij}\phi'_j + C_{ij}\phi_j + D_{ij}\phi'_j) \right\}_{ik} \\ 8\pi\sigma_y(x, y)_i &= \left\{ \left[\ln \left(\frac{\delta_x^2 + \delta_y^2}{4} \right) + \frac{2\delta_x}{\delta_y} \tan^{-1} \frac{\delta_y}{\delta_x} - 1 \right] (gA)_k + \sum_{k=1}^m \left\{ \ln [(x-\xi)^2 + (y-\eta)^2] \right. \right. \\ &\quad \left. \left. + \frac{2(x-\xi)^2}{(x-\xi)^2 + (y-\eta)^2} + 1 \right\} (gA)_k + \sum_{j=1}^n (-A_{ij}\phi_j - B_{ij}\phi'_j + E_{ij}\phi_j + F_{ij}\phi'_j) \right\}_{ik} \\ -8\pi\tau_{xy}(x, y)_i &= \sum_{k=1}^m \left[\frac{2(x-\xi)(y-\eta)}{(x-\xi)^2 + (y-\eta)^2} \right]_{ik} (gA)_k + \sum_{j=1}^n (G_{ij}\phi_j + H_{ij}\phi'_j + I_{ij}\phi_j + K_{ij}\phi'_j) \end{aligned} \right\} \quad (36)$$

where now $i = 1, 2, 3, \dots, m$ refers to the centroid of the i^{th} cell, δ_x and δ_y represent, respectively, x -directional and y -directional dimension of the cell. The coefficients A_{ij} , B_{ij} , C_{ij} , D_{ij} , E_{ij} , F_{ij} , G_{ij} , H_{ij} , I_{ij} , and K_{ij} are obtained by appropriate differentiation under the integral sign of the coefficients given by Eqs. (33) and are listed in Appendix B.

The stress function ϕ is not constant on the loaded boundaries BC and B'C'. The assumption that ϕ is piece-wise constant may lead to appreciable errors in the numerical results. To eliminate this source of error, the summations given in Eqs. (32) and (36) for intervals lying on the loaded boundaries and involving the stress function are replaced by direct integration.

Boundary Interval and Interior Grid Size

The number of nodal points prescribed for the boundary is theoretically unlimited. However, computer storage capacity for the computer used and difficulties associated with inversion of large matrices limited the order of the coefficient matrix [B] of Eq. (35) used herein to 140.

Because of geometric and loading symmetry about the x-axis, it is possible to reduce the number of unknowns. For $2n$ total number of nodal points the number of equations and unknowns ϕ_j and ϕ_j' , is reduced from $4n$ to $2n$. Additional reduction in the number of unknowns is accomplished by taking into consideration St. Venant's effect at the loaded boundaries (Ref. (12)).

Since the vicinity of the crack tip is of greatest interest, a fine nodal spacing along the notch was chosen. To reduce the error introduced by the change in the interval size (Ref. (13)) around boundary points A and A' and at the same time to obtain fine resolution at the tip of the notch, the boundary along the notch was divided into a number of intervals progressively decreasing in length. The rate of change in the interval length and the resulting length of the smallest interval was found to have a great influence on the stress field in the vicinity of the tip of the notch. The rate of change in the interval's length along these boundaries was optimized by the method presented in Ref. (14). For the cases considered optimum ratios of the lengths of two consecutive boundary intervals were found to be in the range of 1.08 to 1.10. The resulting smallest dimensionless boundary interval length varied from 0.0001 to 0.0002. A set of 140 equations containing 140 unknowns was used. Note that the corner points are always designated as interval points, never as nodal points, thus eliminating discontinuous functions from numerical analysis.

The choice of the size of the grid, which has to cover the region where plastic flow is expected to occur, is of utmost importance. A too coarse grid will not detect changes in the values of plastic-strain for small loading increments. A too fine mesh size may result in distorted values of second-order derivatives of plastic strains, which appear in the function $g(x,y)$. The loading increment and the grid size are related to each other. A bad choice of either of them could result in the divergence of the iterative process. To allow the maximum of grid points to be within the expected plastic zone, a variable grid spacing was chosen. The grid used for plane strain conditions was finer, in general, than the one used for plane stress cases.

The interior region, where plastic flow is expected, was divided into $r \times s$ rectangular cells. Due to symmetry about the x-axis, the number of unknown functions g , appearing in the boundary Eqs. (32) and stress Eqs. (36), was reduced from $r \times s$ to $m = r \times (s + 1)/2$, where now the coefficients of these functions represent the sum of the effect of left-hand and right-hand sides of the plastic field. Because of computation time limitations, the grid was arranged in a 27×23 cell pattern, resulting in the number of unknowns g to be equal to 324. By increasing the number of unknowns to 400,

the computation time for one iteration almost doubled. The smallest cells, located in the vicinity of the tip of the notch, have dimensions $\delta_x/w = 0.004$; $\delta_y/w = 0.008$ for plane strain cases, and $\delta_x/w = 0.004$, $\delta_y/w = 0.016$ for plane stress cases.

The solution to the problem was obtained by the method of successive elastic solutions as discussed for the torsion problem and described in detail in Refs. (5) and (15). The computations were performed on a digital computer using a FORTRAN IV program with single-precision arithmetic. The matrix system given by Eq. (35) was solved using the modified Gauss elimination method, which utilizes pivoting and forward and backward substitutions.

Results

A number of beam problems were solved for both plane strain and plane stress cases. These included notch depth to beam depth ratios of 0.3 and 0.5, notch angles of 3° and 10° , strain hardening parameter values of 0.05 and 0.10. In addition, calculations were performed using the actual stress-strain curve of a 5083-0 aluminum alloy. For all cases Poisson's ratio was set at 0.33.

The load increment size used was necessarily a compromise between the accuracy desired and computational time required for convergence. For strain hardening parameter $m = 0.05$ the load increment size $\Delta\tilde{q}$ defined as $\Delta\sigma_{\max}/\sigma_0$ was taken equal to 0.05; while for $m = 0.10$, $\Delta\tilde{q} = 0.10$. For the case of a 5083-0 aluminum alloy, where the actual stress-strain curve was used, the load was incremented by $\Delta\tilde{q} = 0.025$.

For the beam with dimensionless notch depth $\tilde{a} = 0.5$ the minimum load required to produce plastic flow at the most highly stressed grid points was found to be $\tilde{q} = 0.30$, and for $\tilde{a} = 0.3$ the initial load was found to be $\tilde{q} = 0.50$. The maximum load considered was $\tilde{q} = 0.7$ for the $\tilde{a} = 0.5$ cases, and $\tilde{q} = 0.9$ for the $\tilde{a} = 0.3$ cases. In the process of solving the aforementioned problems, the case with strain hardening parameter $m = 0.05$ required approximately 50 iterations for each increment of load (i.e., $\Delta\tilde{q} = 0.05$) for the relatively fine convergence parameter used. For cases where the strain hardening parameter $m = 0.10$ the average number of iterations needed for each increment of load (i.e., $\Delta\tilde{q} = 0.10$) was reduced to 40, while use of the actual stress-strain curve resulted in convergence in approximately 10 iterations for the plane strain case and in 20 iterations for the plane stress case.

Typical results of the computations are presented in Figs. 11 to 18 and Tables V and VI. Complete detailed results are given in Ref. (11).

The growth of the plastic zone with load is shown in Figs. 11 to 14. It is seen that the shapes of the elastoplastic boundaries remain similar to each other as the load increases. As expected, plastic flow starts around the tip of the notch and as the load increases appears also at the boundary opposite the notch. Comparison of Figs. 11 and 12 with Figs. 13 and 14 shows that for the same loads the size of the plastic zones for plane strain are considerably smaller than for plane stress.

In the case of an elastoplastic problem the stress intensity factor K_I must be generalized to the form

$$K_I^*(\sigma_{\max}) = \lim_{r \rightarrow 0} \sqrt{2\pi} \, r^n \sigma_y(r, \theta) \Big|_{\theta=0} \quad (37)$$

where the exponent n is a function of the applied load, σ_{\max} . For linear elastic

behavior K_I is identical with K_I and $n = 1/2$. For the elastoplastic case the variation of n with load is shown in Tables V and VI. In the case of plane strain the stress singularity n decreases slowly as the load increases. For the plane stress case, there is a sudden drop in n from its elastic value as plastic flow appears. Subsequently n slowly increases approaching a limit as the load increases.

Variation of the dimensionless generalized stress intensity factor with load is shown in Fig. 15 for the case of a specimen with notch depth of $\tilde{a} = 0.5$ and $\alpha = 10^\circ$, under plane strain condition and two values of strain hardening parameter m . The stress intensity factor shows no significant increase over the linear elastic value up to an applied load of $\tilde{q} = 0.40$. Above this load K_I increases progressively for both m 's, at the faster rate for the lower strain hardening parameter.

The products of y -directional stress and total strain were also calculated for various cases. The order of singularity of that product was determined by plotting $\ln(\sigma_y \epsilon_y)$ against $\ln r$ and by making a least squares fit of a straight line through the plotted points. It was found to be very close to unity for all cases considered.

The y -directional notch opening displacement was obtained for each case by numerical integration of the relation $\epsilon_{ij} = (1/2)(u_{i,j} + u_{j,i})$ along straight line paths. For each case a number of paths were chosen through the plastic region near the notch, and the resulting displacements were averaged. In general, the notch opening displacement varies linearly with the load until the plastic zone is established at the boundary opposite the notch. Then it increases rapidly, reaching values several times that which would be calculated from the elastic solution.

In order to verify in part the accuracy of the method used, a comparison of notch opening displacements was made with experimental results obtained by Bubsey and Jones (private communication from R. T. Bubsey and M. H. Jones of NASA Lewis Research Center). The specimen used in this experiment, made of aluminum 5083-0 with a length to width ratio of 4 and a crack length $\tilde{a} = 0.5$, was subjected to three-point bending. The stress-strain curve for this specimen is shown in Fig. 16. The experimental results as shown in Fig. 17 are in good agreement with numerical results obtained herein.

Finally, the J integral was evaluated for several cases. As in notch opening displacement calculations, straight line paths were chosen through the plastic zone near the tip of the notch. The integral was evaluated using values of stresses, strains, and displacements at cell centroids for a number of paths. The path independence of J was not conclusive, since the results varied up to 15 percent from the averaged value. It is possible that the results obtained herein do not indicate that the path independent property is lost but rather that the field values of the displacements are not calculated with sufficient accuracy.

The average values of the dimensionless \tilde{J} integral as a function of load are plotted in Fig. 18 for a case of a specimen with a 10° edge notch, $\tilde{a} = 0.5$, $m = 0.05$, and plane strain condition. At the start of plastic flow \tilde{J} increases rapidly with load. This is followed by almost linear variation with additional load.

From the above results it appears that the BIE method applied to the plane problem and formulated in terms of the Airy stress function is capable of giving detailed results such as stress and strain distributions around the tip of the notch and, related to them, the shapes of plastic zones. This was accomplished using a relatively small number of unknowns.

The presence of a singularity at the tip of the notch makes accurate answers very difficult to obtain. Nevertheless good agreement was obtained between the calculated results and experimentally measured notch opening displacement as shown in Fig. 17. Some improvement in the solution techniques and further investigation of the influence of the boundary nodal spacing and interior grid size on the resulting stress and strain fields, and therefore, on the notch opening displacements and J integrals, is still desirable.

THE DISPLACEMENT FORMULATION

Although the biharmonic formulation previously described appears as a viable approach in solving the plane elastoplastic problem, some difficulties are encountered in calculating displacements since numerical differentiations are required in the process which can lead to appreciable errors and inconsistency of results. A more direct formulation of the problem is given in terms of the Navier equilibrium equations for the displacements. The general equations are given in Ref. (4) and several problems using these relations are reported in Ref. (10).

As shown in Ref. (3) the Navier equations with plastic flow can be converted to the BIE

$$\lambda u_i(P) = \int_C (U_{ij}P_j - T_{ij}u_j)dq + \int_R \Sigma_{jki} (\epsilon_{jk}^p + \Delta\epsilon_{jk}^p)dA \quad (38)$$

where u_j and P_j are the boundary displacements and boundary loads, respectively, and the usual tensor notation is used. The tensors U_{ij} , T_{ij} , and Σ_{jki} are given by

$$U_{ij} = C_1(\delta_{ij}C_2 \ln r - r_{,i}r_{,j}) \quad (39)$$

$$T_{ij} = \frac{C_3}{r} \left[\frac{\partial r}{\partial n_q} (\delta_{ij}C_4 + 2r_{,i}r_{,j}) + C_4(r_{,j}n_i - r_{,i}n_j) \right] \quad (40)$$

$$\Sigma_{jki} = \frac{C_3}{r} \left[C_4(\delta_{ij}r_{,k} + \delta_{ki}r_{,j} - \delta_{jk}r_{,i}) + 2r_{,i}r_{,j}r_{,k} \right] \quad (41)$$

with

$$\left. \begin{aligned} C_1 &= -\frac{1}{8\pi G(1-\mu)}, \quad C_2 = 3-4\mu \\ C_3 &= -\frac{1}{4\pi(1-\mu)}, \quad C_4 = 1-2\mu \end{aligned} \right\} \quad (42)$$

and r is the distance from the fixed point P to the variable point of integration, q . The above equations are for the case of plane strain. For plane stress one replaces μ by $\mu/(1+\mu)$. The coefficient λ is equal to 1, if P is an interior point and is equal to 1/2, if $P = p$ is a boundary point.

The solution is now obtained by replacing the integrals by sums as before, resulting in $2n$ simultaneous equations for the case of n boundary segments. These can be written as the matrix equation

$$\begin{bmatrix} A + \frac{1}{2}I & B \\ A' & B' + \frac{1}{2}I \end{bmatrix} \begin{bmatrix} u \\ v \end{bmatrix} = \begin{bmatrix} \gamma \\ \delta \end{bmatrix} + \begin{bmatrix} C \\ D \end{bmatrix} + \begin{bmatrix} \Delta C \\ \Delta D \end{bmatrix} \quad (43)$$

where A , B , A' , and B' are $n \times n$ matrices of known coefficients. u and v are the x and y displacement vectors for the boundary nodal points. γ and δ are vectors given by

$$\left. \begin{aligned} \gamma &= \alpha P_x + \beta P_y \\ \delta &= \alpha' P_x + \beta' P_y \end{aligned} \right\} \quad (44)$$

where α , β , α' , and β' are known $n \times n$ matrices and P_x, P_y are the x and y boundary force vectors at the nodal points. The vectors C and D are functions of the accumulated plastic flow and are known at the beginning of each load increment. The vectors ΔC and ΔD depend on the plastic flow increments during the current load increment and are obtained by iteration. All the terms appearing in Eqs. (43) and (44) are listed in Appendix C.

For the first boundary value problem where the loads are specified over the complete boundary, Eq. (43) is solved directly for the unknown displacements at the boundary nodes. For a mixed boundary value problem, where the displacements at some of the nodes are specified and the loads are unknown at these nodes an obvious interchange of the appropriate columns of the coefficient matrices must be made.

Once Eq. (43) is solved for the unknown displacements (and loads if any), the total strains are computed at any interior point by differentiating Eq. (38) with $\lambda = 1$. At an interior point $P_{ij} \equiv P(x_i, y_j)$ we can write

$$\left. \begin{aligned} \epsilon_x(P_{ij}) &= \sum_{m=1}^n (P_{xm} E_{ijm} + P_{ym} F_{ijm} - u_m G_{ijm} - v_m H_{ijm}) + I_{ij} + \Delta I_{ij} \\ \epsilon_y(P_{ij}) &= \sum_{m=1}^n (P_{xm} E'_{ijm} + P_{ym} F'_{ijm} - u_m G'_{ijm} - v_m H'_{ijm}) + I'_{ij} + \Delta I'_{ij} \\ \epsilon_{xy}(P_{ij}) &= \sum_{m=1}^n (P_{xm} E''_{ijm} + P_{ym} F''_{ijm} - u_m G''_{ijm} - v_m H''_{ijm}) + I''_{ij} + \Delta I''_{ij} \end{aligned} \right\} \quad (45)$$

All the coefficients are given in Appendix C. The plastic strain increments are then computed from the plastic strain-total strain relations and the stress-strain curve as given in Refs. (3,5), the method of successive elastic solutions being used to obtain these strain increments iteratively.

It is shown in Ref. (16), that greater accuracy can be obtained for the same number of nodal points by assuming linear variations of the unknowns on the boundary intervals. This of course complicates to some extent the calculation of the coefficient matrices. Furthermore the nodal points can no longer be taken at the midpoints of the intervals, but must be taken at the end points. This introduces some further complication when a

nodal point occurs at a corner, since firstly, the boundary load may be discontinuous at a corner and secondly, the jump in the boundary integral at a corner is no longer $1/2$, but depends on the corner angle.

Although these additional complications can be taken care of as was done in Ref. (16), a somewhat different but approximately equivalent approach was attempted herein. The nodal points were kept at the centers of the intervals. Each interval was divided into a number of subintervals and the integral for each subinterval was weighted linearly according to its distance from the nodal point. This approximates a linear variation of the unknowns over the intervals.

This approach did indeed give improved results. For example, for the beam of Fig. 7, with $a/w = 0.5$, $L/w = 1.2$, the plane strain elastic maximum crack opening is $E\nu/6M = 5.67$. The value obtained using 90 nodal points was 4.92 assuming constant values over each interval, and was 5.62 using the linear weighting technique.

Results

Calculations were made by the above technique for the same problem as was solved by the biharmonic formulation previously described. Some preliminary results are shown in Figs. 17 and 19. Fig. 17 compares both the biharmonic formulation and the displacement formulation with experimental results for the maximum notch opening. The biharmonic and displacement formulations give results which are in very good agreement. The same is seen in Fig. 19 where the stress σ_y at a value of x very close to the notch tip is plotted against the distance from the notch centerline, y . The agreement between the two formulations is again very good. The calculations for larger load increments using the displacement formulation have not yet been carried out. These are presently under way.

A preliminary comparison of the convergence rate of the two formulations indicates that the plastic flow computations converge more rapidly using the displacement formulation. A comparison of the computer times, however, could not be made, since the two types of calculation were carried out on different computers.

CONCLUDING REMARKS

This preliminary survey of the use of BIE methods for elastoplastic problems indicates that they form a viable and worthwhile approach for solving such problems. The torsion problem in particular can easily be solved for almost any geometry cross section.

The plane elastoplastic problem can be solved by using either a biharmonic formulation or a displacement formulation. Both appear to give good results with relatively small sets of equations, even for problems with singularities, such as beams with notches.

Although no comparison was made herein with the finite element method, such comparisons were made in Ref. (16). It is indicated in Ref. (16) that the computer times for the finite element method and BIE method (using the displacement formulation) are comparable. Finer resolution can however be obtained by the BIE method.

The application of the BIE method to elastoplastic problems is still in its early stages. Much work remains to be done in refining the techniques for optimum application.

APPENDIX A

BOUNDARY INTEGRAL COEFFICIENTS FOR TORSION PROBLEM

The division of the boundary into intervals with their corresponding nodal points is shown in Fig. 20. The x and y coordinates of a boundary nodal point p_i are designated as (x_{bi}, y_{bi}) . The coordinates at the beginning and end of an interval (say interval j) are designated by (ξ_j, η_j) at the beginning of the interval and by (ξ_{j+1}, η_{j+1}) at the end of the interval. The interval lengths h_j need not be equal. The coordinates of the centroid of an interior cell where plastic flow occurs are designated by (x_k, y_k) .

The coefficients in Eq. (13) are then given by

$$\left. \begin{aligned} a_{ij} &= \int_{q_{j-(1/2)}}^{q_{j+(1/2)}} \frac{\partial}{\partial n_q} (\ln r_{p_i q}) dq \\ &\approx h_j \frac{(x_{bj} - x_{bi})\xi_j + (y_{bj} - y_{bi})\eta_j}{r_{ij}^2} \quad j \neq i \\ a_{ii} &= \pi - \sum_{k \neq i} a_{ik} \end{aligned} \right\} \quad (46)$$

The last relation follows from the Gaussian condition, that is,

$$\int_C \frac{\partial}{\partial n_q} \ln r_{pq} dq = \pi$$

To evaluate the b_{ij} coefficients Simpson's rule is used for the case $i \neq j$ and closed form integration is used for the case $i = j$ since the integrand is singular for $i = j$. The result is

$$\left. \begin{aligned} b_{ij} &= \frac{h_j}{6} \ln \left[r_{i, j-(1/2)} + \frac{1}{2} \ln r_{ij} + \ln r_{i, j+(1/2)} \right] \quad i \neq j \\ b_{ii} &= h_i \left(\ln \frac{h_i}{2} - 1 \right) \end{aligned} \right\} \quad (47)$$

$$R_i = -\frac{1}{4} \sum_{k, \ell} F_{k\ell} \ln r_{ik\ell} \Delta A_{k\ell} \quad (48)$$

where $\sum_{k, \ell}$ is the sum for all the plastic cells in the region and $\Delta A_{k\ell}$ is the area of the cell with coordinates (x_k, y_k) .

The coefficients A_{ijk} , B_{ijk} , C_{ijk} , and D_{ijk} are given as follows using Simpson's rule:

$$A_{ijk} = \frac{h_k}{6} \left\{ \frac{(x_i - \xi_k)^2 - (y_j - \eta_k)^2}{r_{ij, k-(1/2)}^4} + 4 \frac{(x_i - x_{bk})^2 - (y_j - y_{bk})^2}{r_{ijk}^4} + \frac{(x_i - \xi_{k+1})^2 - (y_j - \eta_{k+1})^2}{r_{ij, k+(1/2)}^4} \right\} \quad (49)$$

$$B_{ijk} = \frac{h_k}{3} \left\{ \frac{(x_i - \xi_k)(y_j - \eta_k)}{r_{ij, k-(1/2)}^4} + 4 \frac{(x_i - x_{bk})(y_j - y_{bk})}{r_{ijk}^4} + \frac{(x_i - \xi_{k+1})(y_j - \eta_{k+1})}{r_{ij, k+(1/2)}^4} \right\} \quad (50)$$

$$C_{ijk} = \frac{h_k}{6} \left[\frac{x_i - \xi_k}{r_{ij, k-(1/2)}^2} + 4 \frac{x_i - x_{bk}}{r_{ijk}^2} + \frac{x_i - \xi_{k+1}}{r_{ij, k+(1/2)}^2} \right] \quad (51)$$

$$D_{ijk\ell} = \frac{x_i - x_k}{(x_i - x_k)^2 + (y_j - y_\ell)^2} \Delta A_{k\ell} \quad (52)$$

APPENDIX B

COEFFICIENTS OF THE STRESS EQUATIONS (36)

The coefficients appearing in stress Eqs. (36) are given by the following relations:

$$\begin{aligned}
 A_{ij} - \frac{\partial^2}{\partial y^2} (e_{ij}) &= 4 \int_j \frac{\partial}{\partial n} \left\{ \frac{(x_1 - \xi)^2 - (y_1 - \eta)^2}{[(x_1 - \xi)^2 + (y_1 - \eta)^2]^2} \right\} dq \\
 B_{ij} - \frac{\partial^2}{\partial y^2} (f_{ij}) &= 4 \int_j \frac{(y_1 - \eta)^2 - (x_1 - \xi)^2}{[(x_1 - \xi)^2 + (y_1 - \eta)^2]^2} dq \\
 C_{ij} - \frac{\partial^2}{\partial y^2} (c_{ij}) &= \int_j \frac{\partial}{\partial n} \left\{ \ln [(x_1 - \xi)^2 + (y_1 - \eta)^2] + \frac{2(y_1 - \eta)^2}{(x_1 - \xi)^2 + (y_1 - \eta)^2} \right\} dq \\
 D_{ij} - \frac{\partial^2}{\partial y^2} (d_{ij}) &= - \int_j \left\{ \ln [(x_1 - \xi)^2 + (y_1 - \eta)^2] + \frac{2(y_1 - \eta)^2}{(x_1 - \xi)^2 + (y_1 - \eta)^2} + 1 \right\} dq \\
 E_{ij} - \frac{\partial^2}{\partial x^2} (c_{ij}) &= \int_j \frac{\partial}{\partial n} \left\{ \ln [(x_1 - \xi)^2 + (y_1 - \eta)^2] + \frac{2(x_1 - \xi)^2}{(x_1 - \xi)^2 + (y_1 - \eta)^2} \right\} dq \\
 F_{ij} - \frac{\partial^2}{\partial x^2} (d_{ij}) &= - \int_j \left\{ \ln [(x_1 - \xi)^2 + (y_1 - \eta)^2] + \frac{2(x_1 - \xi)^2}{(x_1 - \xi)^2 + (y_1 - \eta)^2} + 1 \right\} dq \\
 G_{ij} - \frac{\partial^2}{\partial x \partial y} (e_{ij}) &= -8 \int_j \frac{\partial}{\partial n} \left\{ \frac{(x_1 - \xi)(y_1 - \eta)}{[(x_1 - \xi)^2 + (y_1 - \eta)^2]^2} \right\} dq
 \end{aligned} \tag{53}$$

(continued)

$$\begin{aligned}
 H_{ij} &= \frac{\partial^2}{\partial x \partial y} (f_{ij}) = 2 \int_j \frac{(x_1 - \xi)(y_1 - \eta)}{[(x_1 - \xi)^2 + (y_1 - \eta)^2]^2} d\eta \\
 I_{ij} &= \frac{\partial^2}{\partial x \partial y} (c_{ij}) = 2 \int_j \frac{\partial}{\partial \eta} \left[\frac{(x_1 - \xi)(y_1 - \eta)}{(x_1 - \xi)^2 + (y_1 - \eta)^2} \right] d\eta \\
 K_{ij} &= \frac{\partial^2}{\partial x \partial y} (d_{ij}) = -2 \int_j \frac{(x_1 - \xi)(y_1 - \eta)}{(x_1 - \xi)^2 + (y_1 - \eta)^2} d\eta
 \end{aligned}
 \tag{53}$$

The evaluation of these integrals is given in Ref. (11).

APPENDIX C

COEFFICIENTS OF DISPLACEMENT FORMULATION EQUATIONS

The coefficients appearing in Eqs. (43) to (45) are given as follows:

Let

$$\left. \begin{aligned}
 E_1 &= \theta \Big|_m^{m+1} \\
 E_2 &= \sin \theta \cos \theta \Big|_m^{m+1} \\
 E_3 &= \sin^2 \theta \Big|_m^{m+1} \\
 E_5 &= \ln r \Big|_m^{m+1} \\
 E_6 &= \cos^4 \theta \Big|_m^{m+1} \\
 E_7 &= \sin^4 \theta \Big|_m^{m+1} \\
 E_8 &= \tan \theta \ln r \Big|_m^{m+1} \\
 E_9 &= \tan \theta \Big|_m^{m+1} \\
 D &= r_m \cos \theta_m
 \end{aligned} \right\} \quad (54)$$

where

$$\theta_m = \sin^{-1} \left(\ln \frac{y_m - y_l}{r_{lm}} - m_m \frac{x_m - x_l}{r_{lm}} \right)$$

Then

$$\begin{aligned}
A_{ij} &= C_3[(C_4 + 1)E_1 + (\ell^2 - m^2)E_2 - 2\ell m E_3] \\
B_{ij} &= C_3[2\ell m E_2 + (\ell^2 - m^2)E_3 + C_4 E_5] \\
\Lambda_{ij} &= C_3[2\ell m E_2 + (\ell^2 - m^2)E_3 - C_4 E_5] \\
B'_{ij} &= C_3[(C_4 + 1)E_1 - (\ell^2 - m^2)E_2 + 2\ell m E_3] \\
\alpha_{ij} &= DC_1[(C_2 - (\ell^2 - m^2))E_1 - (C_2 + m^2)E_9 + 2\ell m E_5 + C_2 E_8] \\
\beta_{ij} &= \alpha'_{ij} = DC_1[-2\ell m E_1 + \ell m E_9 - (\ell^2 - m^2)E_5] \\
\beta'_{ij} &= C_1 D[(C_2 + \ell^2 - m^2)E_1 - (C_2 + \ell^2)E_9 - 2\ell m E_5 + C_2 E_8]
\end{aligned} \tag{55}$$

$$\begin{aligned}
E_{ijm} &= -C_1[(C_2 - (\ell^2 - m^2))\ell E_1 + (\ell^3 - 3\ell m^2)E_2 \\
&\quad + (m^3 - 3m\ell^2)E_3 - m(C_2 - 2\ell^2)E_5] \\
F_{ijm} &= -C_1[-2\ell^2 m E_1 - (m^3 - 3\ell^2 m)E_2 + (\ell^3 - 3\ell m^2)E_3 - \ell(\ell^2 - m^2)E_5] \\
E'_{ijm} &= -C_1[-2\ell m^2 E_1 - (\ell^3 - 3\ell m^2)E_2 - (m^3 - 3\ell^2 m)E_3 - m(\ell^2 - m^2)E_5] \\
F'_{ijm} &= -C_1[(C_2 + \ell^2 - m^2)m E_1 + (m^3 - 3\ell^2 m)E_2 \\
&\quad - (\ell^3 - 3\ell m^2)E_3 + \ell(C_2 - 2m^2)E_5] \\
E''_{ijm} &= -C_1[(C_4 - (\ell^2 - m^2))m E_1 - (m^3 - 3\ell^2 m)E_2 \\
&\quad + (\ell^3 - 3\ell m^2)E_3 + \ell(C_4 + 2m^2)E_5] \\
F''_{ijm} &= -C_1[(C_4 + \ell^2 - m^2)\ell E_1 - (\ell^3 - 3\ell m^2)E_2 \\
&\quad + (m^3 - 3\ell m^2)E_3 - m(C_4 + 2\ell^2)E_5] \\
G_{ijm} &= -\frac{C_3}{D}[(1 - 6\ell^2 - C_4)\ell E_2 + (C_4 - 2 + 10\ell^2)m E_3 \\
&\quad + 2\ell(4\ell^2 - 3)E_4 + 2m(4m^2 - 3)E_7]
\end{aligned} \tag{56}$$

(continued)

$$\left. \begin{aligned}
H_{ijm} &= -\frac{C_3}{D} \left[(2 - 6l^2 - C_4)mE_2 + (-C_4 - 2 + 10m^2)lE_3 \right. \\
&\quad \left. - 2m(4m^2 - 3)E_4 + 2l(4l^2 - 3)E_7 \right] \\
G_{ijm} &= -\frac{C_3}{D} \left[(2 - 6m^2 - C_4)lE_2 + (-C_4 - 2 + 10l^2)mE_3 \right. \\
&\quad \left. - 2l(4l^2 - 3)E_4 + 2m(4m^2 - 3)E_7 \right] \\
H_{ijm} &= -\frac{C_3}{D} \left[(4 - 6m^2 - C_4)mE_2 - (C_4 - 2 + 10m^2)lE_3 \right. \\
&\quad \left. + 2m(4m^2 - 3)E_4 - 2l(4l^2 - 3)E_7 \right] \\
G_{ijm} &= -\frac{C_3}{D} \left[m(6m^2 - 5)E_2 + l(10m^2 - 3)E_3 - 2m(4m^2 - 3)E_4 + 2l(4l^2 - 3)E_7 \right] \\
H_{ijm} &= -\frac{C_3}{D} \left[l(6l^2 - 5)E_2 + m(3 - 10l^2)E_3 - 2l(4l^2 - 3)E_4 - 2m(4m^2 - 3)E_7 \right]
\end{aligned} \right\} \quad (56)$$

and

$$\left. \begin{aligned}
I_{ij} &= \sum_{kl} \left[s_{1111}(P_{ij}, Q_{kl}) \epsilon_x^P(Q_{kl}) + s_{1122}(P_{ij}, Q_{kl}) \epsilon_y^P(Q_{kl}) \right. \\
&\quad \left. + 2 s_{1112}(P_{ij}, Q_{kl}) \epsilon_{xy}^P(Q_{kl}) \right] \Delta A_{kl} \\
I_{ij} &= \sum_{kl} (s_{2211} \epsilon_x^P + s_{2222} \epsilon_y^P + 2 s_{2212} \epsilon_{xy}^P) \Delta A_{kl} \\
I_{ij} &= \sum_{kl} (s_{1211} \epsilon_x^P + s_{1222} \epsilon_y^P + 2 s_{1212} \epsilon_{xy}^P) \Delta A_{kl}
\end{aligned} \right\} \quad (57)$$

and

$$s_{ijk\ell} = \frac{1}{2} \left[\frac{\partial}{\partial x_j} \int_{A_{k\ell}} \sum_{kl i} + \frac{\partial}{\partial x_i} \int_{A_{k\ell}} \sum_{kl j} \right] dA \quad (58)$$

where $k\ell$ represents an interior cell.

If the nodal point i and the integration interval j are on the same straight segment of the boundary, then $D = 0$ and $\theta = \pm \pi/2$, where the plus sign is used when j is ahead of i , and the minus sign is used when j is behind i . This leads to $0 \times \infty$ in the calculation of β_{ij} and β_{ij} . A simple limiting process shows that for this case, with $i \neq j$,

$$\left. \begin{aligned} \beta_{ij} &= \pm C_1 \ell_j m_j (r_{j+1} - r_j) \\ \beta_{ij} &= \pm C_1 \left[C_2 (r_{j+1} \ln r_{j+1} - r_j \ln r_j) - (C_2 + \ell_j^2) (r_{j+1} - r_j) \right] \end{aligned} \right\} \quad (59)$$

and for $i = j$

$$\left. \begin{aligned} \beta_{ij} &= 2C_1 \ell_j m_j r_{j+1} \\ \beta_{ij} &= 2C_1 \left[C_2 r_{j+1} \ln r_{j+1} - (C_2 + \ell_j^2) r_{j+1} \right] \end{aligned} \right\} \quad (60)$$

REFERENCES

1. Symm, G. T., "Integral Equation Methods in Elasticity and Potential Theory," Report prepared for National Physics Lab., MA-51, 1964.
2. Rizzo, F. J., "An Integral Equation Approach to Boundary Value Problems of Classical Elastostatics," Quart. Appl. Math., Vol. 25, Apr. 1967, p. 83.
3. Mendelson, A., "Boundary-Integral Methods in Elasticity and Plasticity," NASA TN D 7418, 1973.
4. Swedlow, J. L. and Cruse, T. A., "Formulation of Boundary Integral Equations for Three-Dimensional Elasto-Plastic Flow," Int. J. Solids Structures, Vol. 7, 1971, p. 1673.
5. Mendelson, A., Plasticity: Theory and Application. Macmillan, New York, 1968.
6. Mendelson, A., "Solution of Elastoplastic Torsion Problem by Boundary Integral Method," NASA TN D 7872, 1975.
7. Prager, W., "An Introduction to the Mathematical Theory of Plasticity," J. Appl. Phys., Vol. 18, Apr. 1947, p. 375.
8. Huth, J. H., "A Note on Plastic Torsion," J. Applied Mech., vol. 22, Sept. 1955, p. 432.
9. Sokolnikoff, I. S., Mathematical Theory of Elasticity, 2nd ed., McGraw-Hill, New York, 1956.
10. Mendelson, A., "Elastic-Plastic Torsion Problems for Strain-Hardening Materials," NASA TN D 4391, 1968.
11. Rzasnicki, W., "Plane Elasto-Plastic Analysis of V-notched Plate Under Bending by Boundary Integral Equation Method," Ph.D. Thesis, Univ. of Toledo, 1973.
12. Gross, B., "Some Plane Problem Elastostatic Solutions for Plates Having a V-Notch," Ph.D. Thesis, Case Western Reserve University, 1970.
13. Walker, G. E., Jr., "A Study of the Applicability of the Method of Potential to Inclusions of Various Shapes in Two- and Three-Dimensional Elastic and Thermo-Elastic Stress Fields," Ph.D. Thesis, Univ. of Washington, 1969.
14. Rzasnicki, W., Mendelson, A., and Albers, L. U., "Application of Boundary Integral Method to Elastic Analysis of V-Notched Beams," NASA TN D 7424, 1973.
15. Rzasnicki, W., Mendelson, A., Albers, L. U., and Raftopoulos, D. D., "Application of Boundary Integral Method to Elastoplastic Analysis of V-Notched Beams," NASA TN D 7637, 1974.
16. Ricciardella, P. C., "An Implementation of the Boundary-Integral Technique for Planar Problems in Elasticity and Elasto-Plasticity," Ph.D. Thesis, Carnegie-Mellon Univ., 1973.

TABLE I. - COMPARISON OF VALUES OF DIMENSIONLESS WARPING FUNCTION ON BOUNDARY
OF ELASTIC SQUARE PLATE WITH EXACT ELASTIC SOLUTION

Boundary value, y	Exact warping function, w	Value of warping function by boundary integral method				Boundary value, y	Exact warping function, w	Value of warping function by boundary integral method				
		Intervals, n						Intervals, n				
		4	8	12	16			4	8	12	16	
0.03125	0.01095	0.04311	0.02184	0.01459	0.01095	0.4313	0.1424	0.1446	0.1446	0.1433	0.1424	
.04167	.01459					.5417	.1433					
.0625	.02185					.5625	.1448					
.09375	.03264					.5938	.1461					
.1250	.04328					.6250	.1461					
.1563	.05374					.6563	.1449					
.1875	.06390					.6875	.1422					
.2083	.07060					.7083	.1396					
.2188	.07380					.7188	.1380					
.2813	.09235					.7813	.1244					
.2917	.09527		.7917	.1214								
.3125	.1009	.1159	.1009	.1090	.8125	.1148	.08826	.08826	.08811	.07129		
.3438	.1090					.8438					.1029	
.3750	.1165					.8750					.08864	
.4063	.1233					.9063					.07166	
.4375	.1293					.9375					.05169	
.4583	.1329					.9583					.03644	
.4688	.1346					.9688					.02808	

TABLE II. - COMPARISON OF ELASTIC SOLUTIONS FOR MAXIMUM
DIMENSIONLESS SHEAR STRESS AND DIMENSIONLESS
MOMENT FOR SQUARE BAR

	Exact solution	Finite difference method (55 eqs.)	Boundary integral method	
			Intervals, n	
			4	8
Dimensionless moment, M^*	1.125	1.122	1.128	1.127
Dimensionless maximum shear stress, τ_{\max}	.6754	.6725	.6724	.6747

TABLE IV. - SUMMARY OF RESULTS FOR TORSION
OF SQUARE PRISMATIC BAR

Linear strain-hardening parameter, m	Dimensionless angle of twist (per unit length), β	Dimensionless moment, M^*	Maximum dimensionless shear stress, τ_{\max}	Maximum dimensionless strain, $\gamma_{\max} \frac{p}{\epsilon_0}$
0	2	1.81	0.751	0.792
	3	1.96	↓	1.70
	4	2.02		2.57
	5	2.06		3.42
	6	2.08		4.25
0.05	2	1.83	0.784	0.758
	3	2.04	.822	1.57
	4	2.15	.852	2.35
	5	2.24	.893	3.12
	6	2.31	.926	3.85
0.10	2	1.85	0.817	0.687
	3	2.11	.890	1.45
	4	2.27	.960	2.17
	5	2.41	1.03	2.86
	6	2.53	1.09	3.52
0.20	2	1.90	0.879	0.593
	3	2.25	1.02	1.24
	4	2.51	1.15	1.85
	5	2.74	1.28	2.43
	6	2.95	1.40	3.00

TABLE III. - COMPARISON OF ELASTIC SOLUTIONS
FOR DIMENSIONLESS x DIRECTIONAL SHEAR

STRESS DISTRIBUTION τ_x

[first number, exact; second, boundary integral method; third, finite difference method.]

y	x						
	0	0.2	0.4	0.6	0.8	1.0	
Elastic solutions							
1.0	0.675 .675 .671	0.658 .658 .654	0.605 .605 .600	0.507 .506 .500	0.342 .339 .330	0	↓
0.8	0.492 .492 .492	0.476 .476 .476	0.427 .427 .428	0.338 .338 .339	0.198 .199 .200	0	↓
0.6	0.339 .339 .340	0.326 .326 .327	0.287 .287 .288	0.219 .220 .220	0.121 .122 .123	0	↓
0.4	0.212 .212 .212	0.203 .203 .203	0.176 .177 .177	0.132 .132 .133	0.0714 .0717 .0720	0	↓
0.2	0.101 .101 .102	0.0971 .0971 .0973	0.0839 .0840 .0842	0.0623 .0624 .0626	0.0333 .0335 .0336	0	↓

TABLE V. - ORDER OF STRESS SINGULARITY n AT THE TIP OF THE NOTCH
FOR A SPECIMEN WITH A SINGLE EDGE NOTCH SUBJECTED TO
PURE BENDING - PLANE STRAIN
[Poisson's ratio $\nu = 0.33$]

Dimensionless notch depth, \tilde{a}	Notch angle, α , deg	Strain hardening parameter, m	Elastic	Dimensionless load, \tilde{q}					
				0.4	0.5	0.6	0.7	0.8	0.9
0.3	3	0.10	0.4099	-----	0.468	0.490	0.487	0.473	0.475
.3	10	.10	↓	-----	.496	.497	.492	.480	.487
.5	10	.05		0.499	.496	480	472	-----	-----
5	10	.10		.496	490	480	.478	-----	-----

TABLE VI. - ORDER OF STRESS SINGULARITY n
AT THE TIP OF THE NOTCH FOR A SPECIMEN
WITH A SINGLE EDGE NOTCH SUBJECTED
TO PURE BENDING - PLANE STRESS

[Dimensionless notch depth $\tilde{a} = 0.3$; notch angle $\alpha = 10^\circ$; strain hardening parameter $m = 0.10$; Poisson's ratio $\nu = 0.33$.]

Elastic	Dimensionless load, \tilde{q}				
	0.5	0.6	0.7	0.8	0.9
0.4999	0.419	0.434	0.448	0.451	0.458

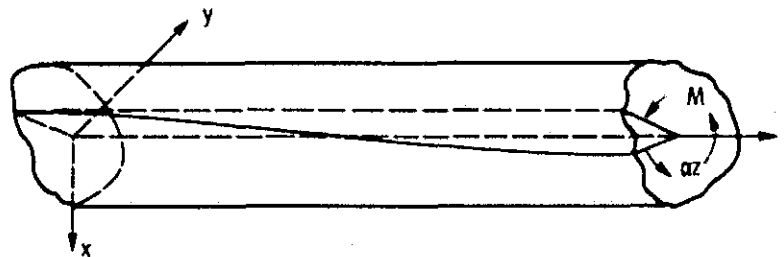


Figure 1. - Prismatic bar subject to twisting couple.

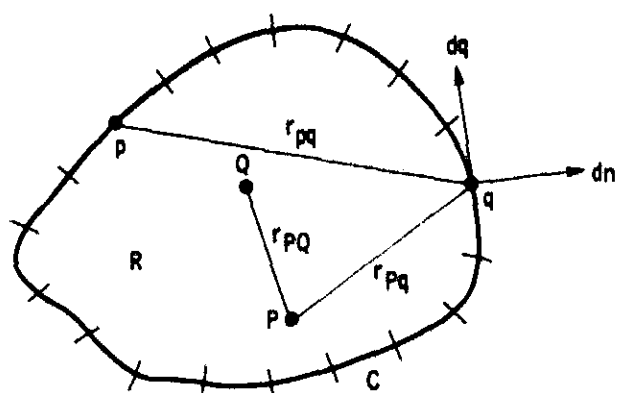


Figure 2. - Region R , boundary curve c , and geometric quantities entering into boundary integrals.

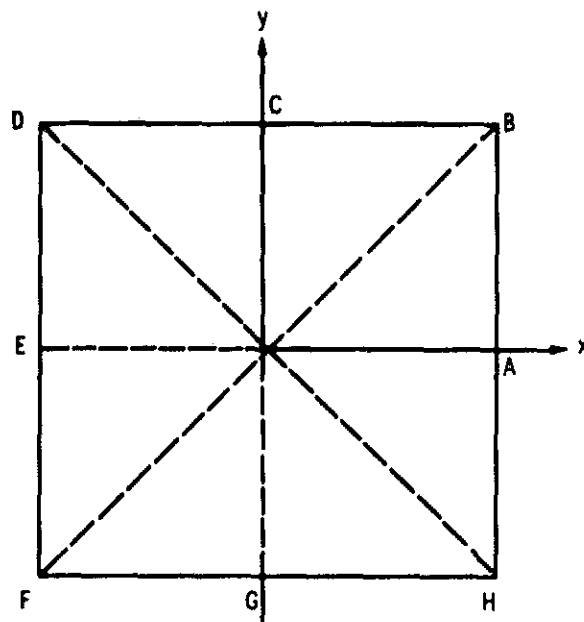


Figure 3. - Square cross section.

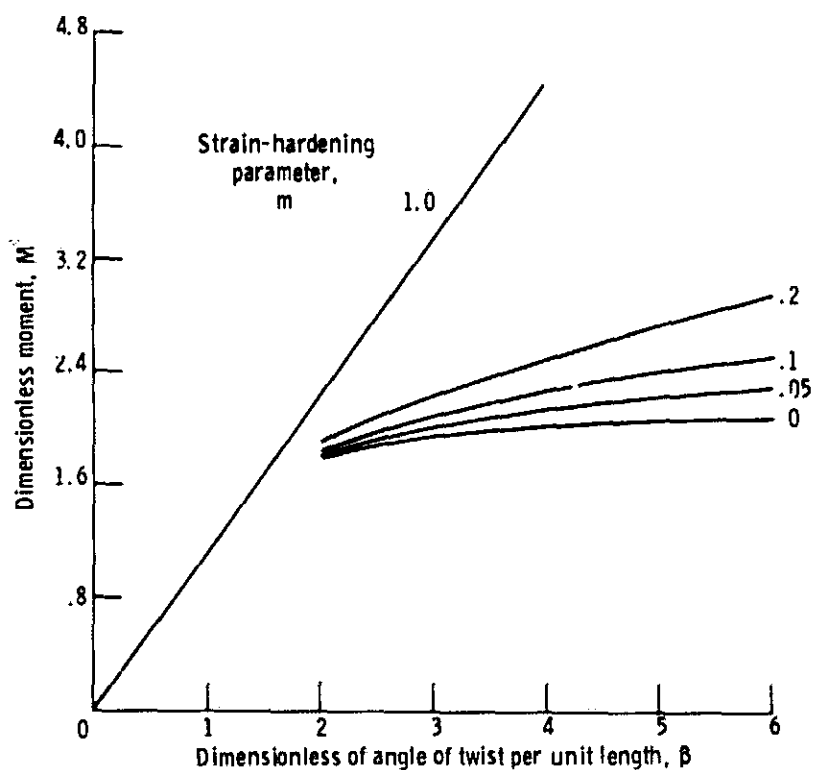


Figure 4. - Variation of dimensionless moment with dimensionless angle of twist per unit length for several values of strain-hardening parameter for square cross section.

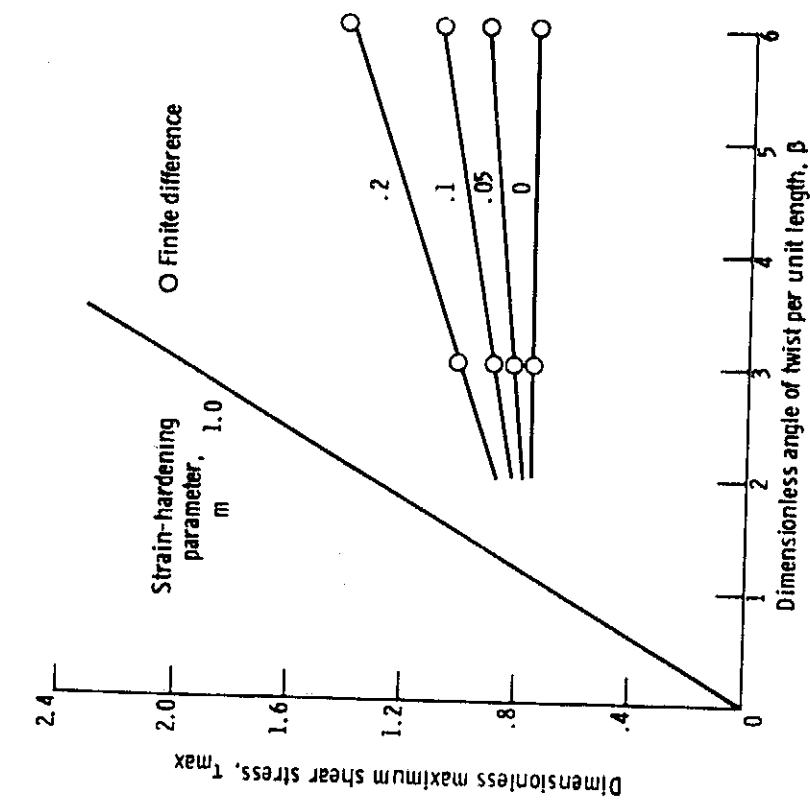


Figure 5. - Variation of dimensionless maximum shear stress with dimensionless angle of twist per unit length for square cross section. Strain-hardening parameter for square cross section.

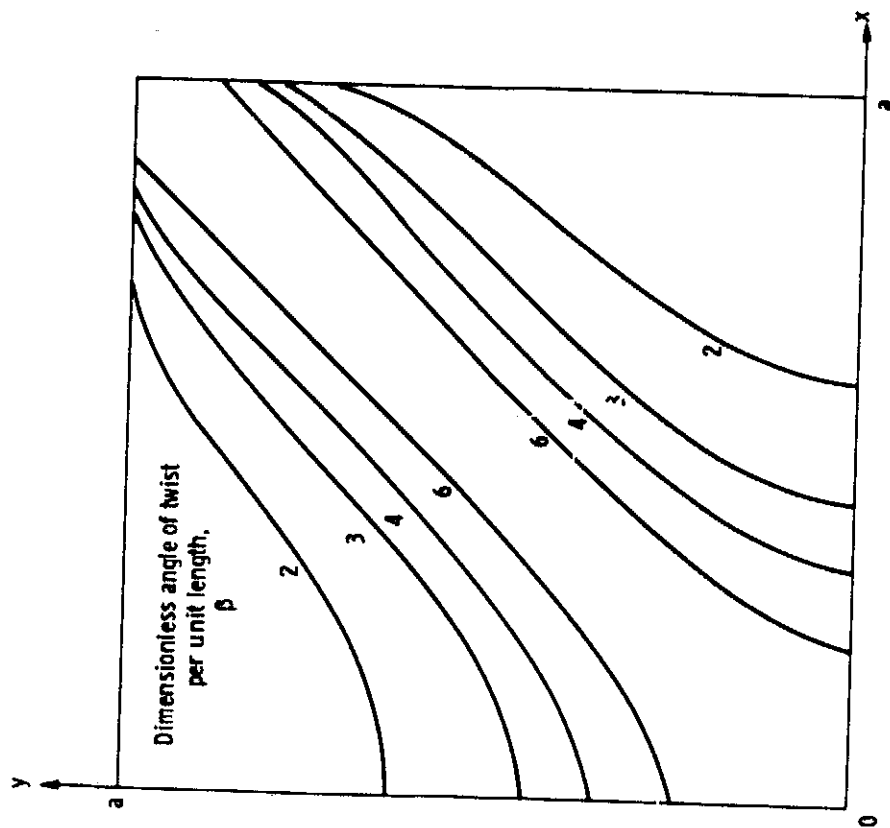


Figure 6. - Plastic zone boundaries in quadrant of square cross section as function of dimensionless angle of twist per unit length for strain-hardening parameter, 0.1.

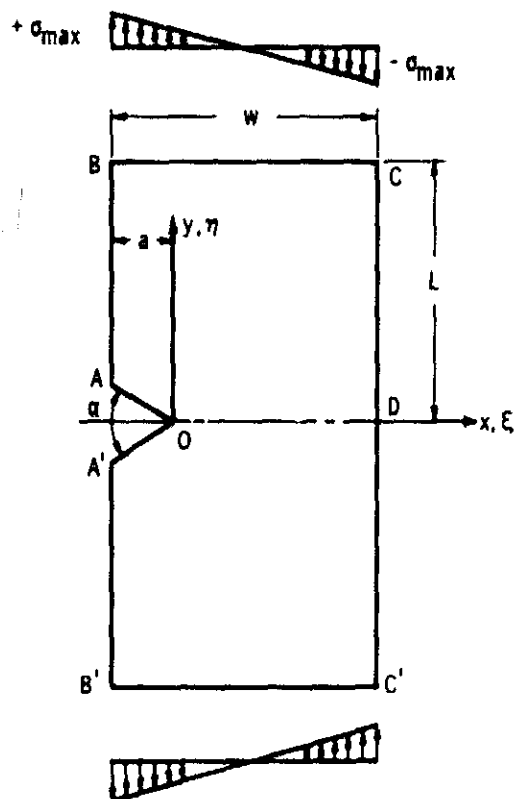


Figure 7. - Single-edge V-notched beam subject to pure bending load.

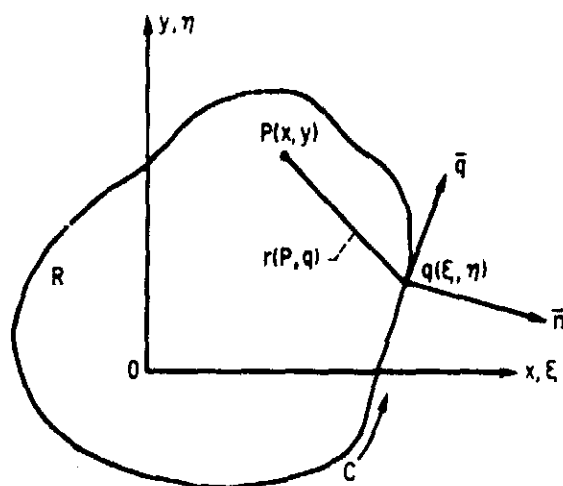


Figure 8. - Sign convention for simply connected region R.

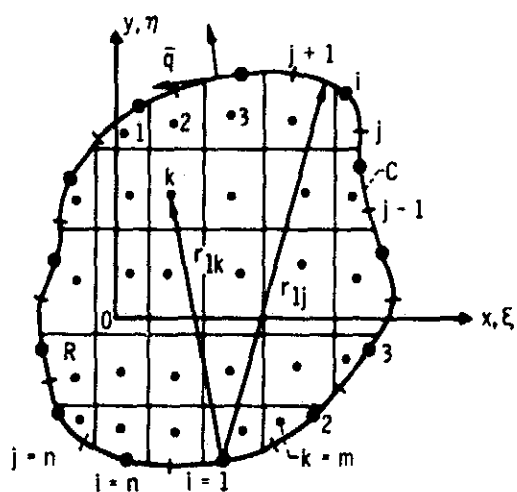


Figure 9. - Boundary and interior region subdivisions for $P(x, y) < C$.

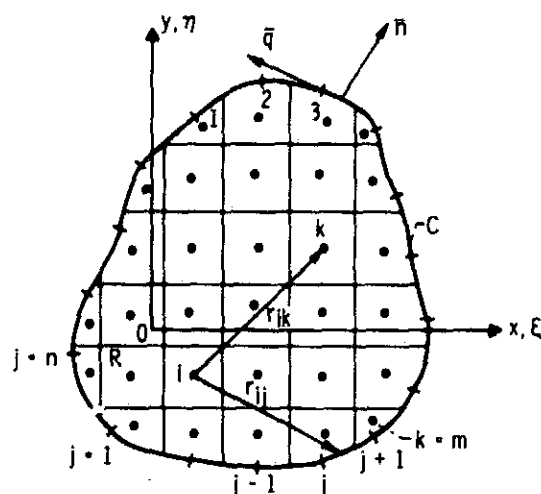


Figure 10. - Boundary and interior region subdivisions for $P(x, y) < R$.

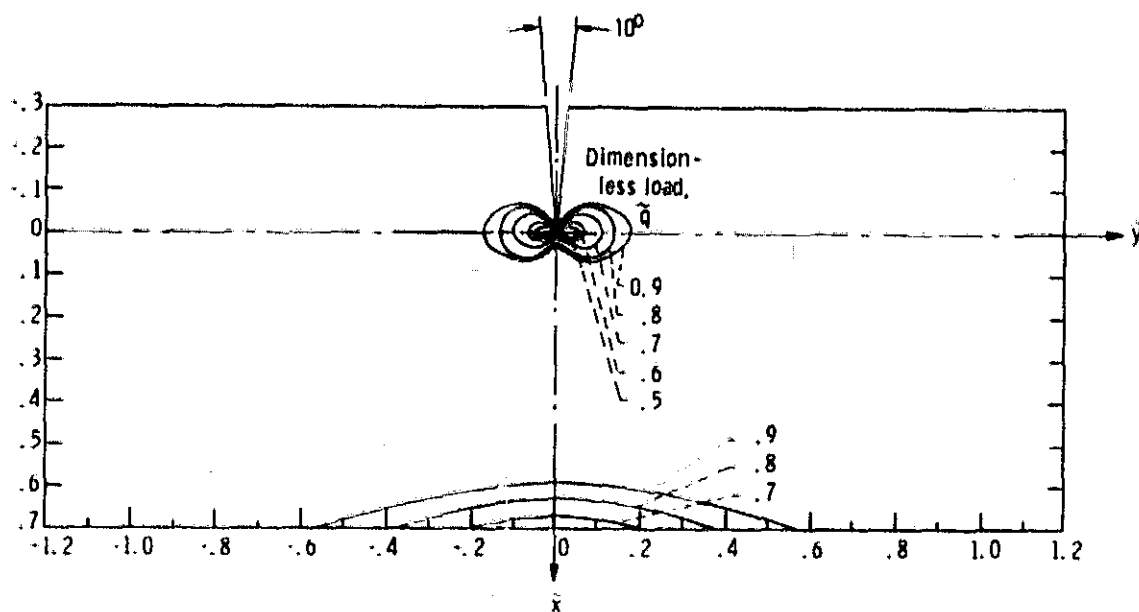


Figure 11. - Growth of plastic zone size with load for specimen with single edge notch subjected to pure bending. Plane strain; dimensionless notch depth $\tilde{a} = 0.3$; notch angle $\alpha = 10^\circ$; strain hardening parameter $m = 0.10$; Poisson's ratio $\mu = 0.33$.

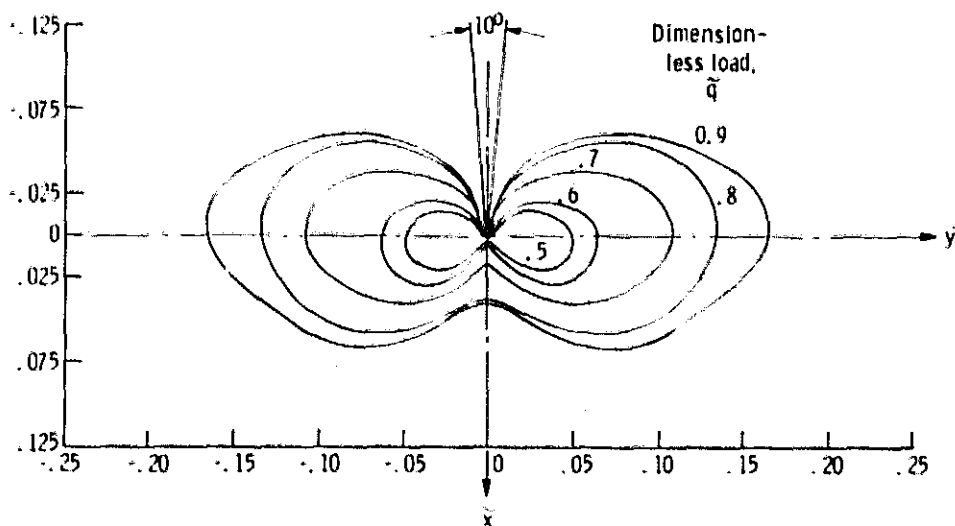


Figure 12. - Growth of plastic zone size with load in vicinity of notch for specimen with single edge notch subjected to pure bending. Plane strain; dimensionless notch depth $\tilde{a} = 0.3$; notch angle $\alpha = 10^\circ$; strain hardening parameter $m = 0.10$; Poisson's ratio $\mu = 0.33$.

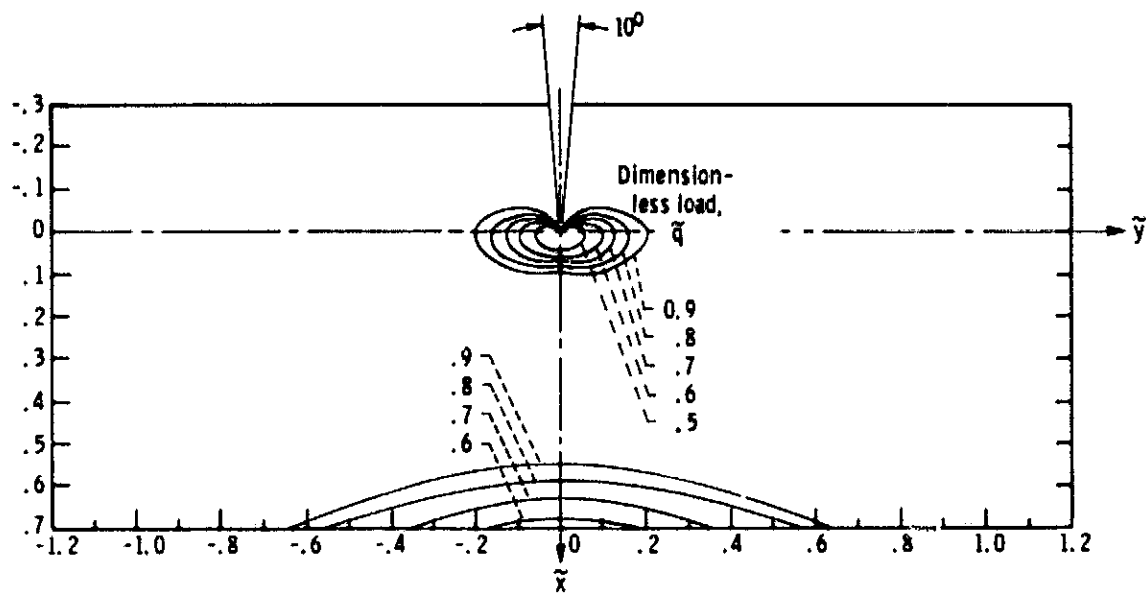


Figure 13. - Growth of plastic zone size with load for specimen with single edge notch subjected to pure bending. Plane stress; dimensionless notch depth $\tilde{a} = 0.3$; notch angle $\alpha = 10^\circ$; strain hardening parameter $m = 0.10$; Poisson's ratio $\mu = 0.33$.

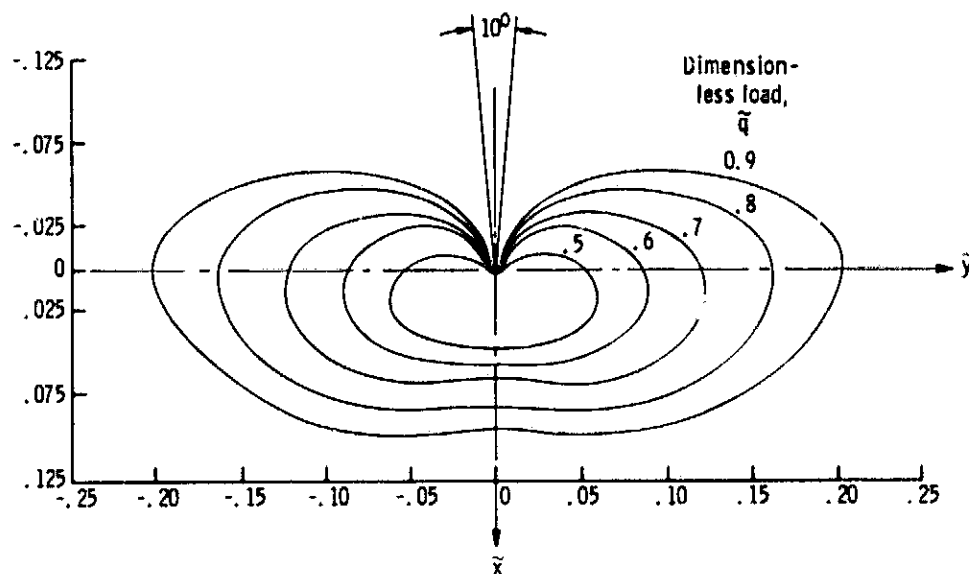


Figure 14. - Growth of plastic zone size with load in vicinity of notch for a specimen with single edge notch subjected to pure bending. Plane stress; dimensionless notch depth $\tilde{a} = 0.3$; notch angle $\alpha = 10^\circ$; strain hardening parameter $m = 0.10$; Poisson's ratio $\mu = 0.33$.

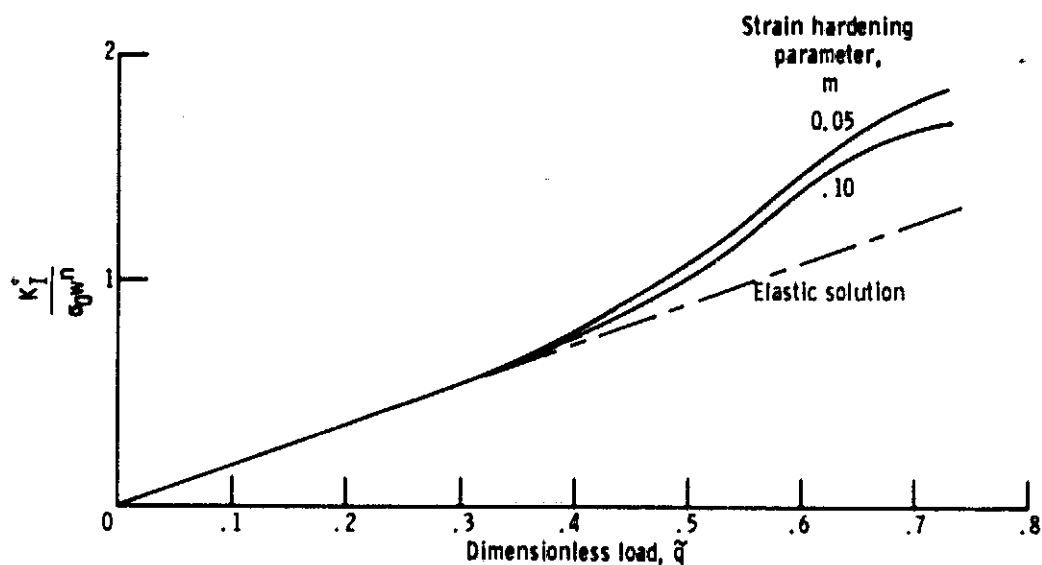


Figure 15. - Variation of dimensionless generalized stress intensity factor with load for specimen with single edge notch subjected to pure bending. Plane strain; dimensionless notch depth $\tilde{a} = 0.5$; notch angle $\alpha = 10^\circ$; Poisson's ratio $\mu = 0.33$.

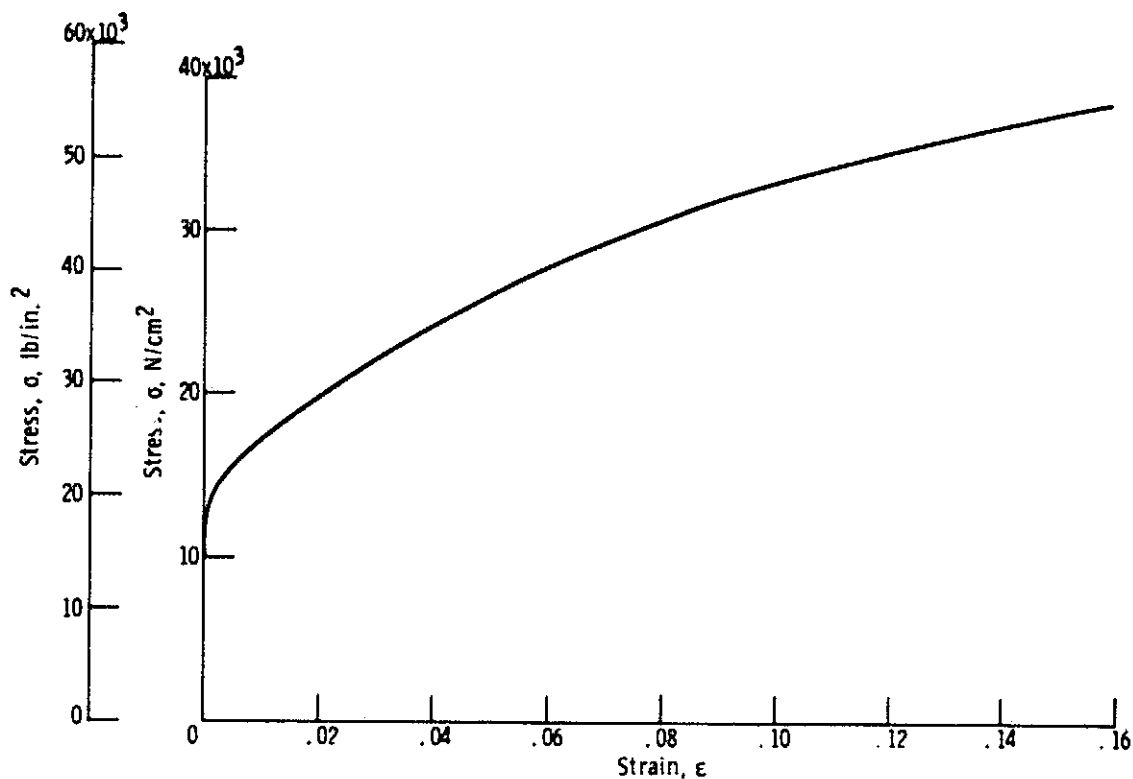


Figure 16. - Stress-strain curve for aluminum 5083-0 used in test (private communication from R. T. Bubsey and M. H. Jones of NASA Lewis Research Center). Young's modulus of elasticity $E = 7.79 \times 10^6$ newtons per square centimeter (11.3×10^6 lb/in.²); Poisson's ratio $\mu = 0.33$.

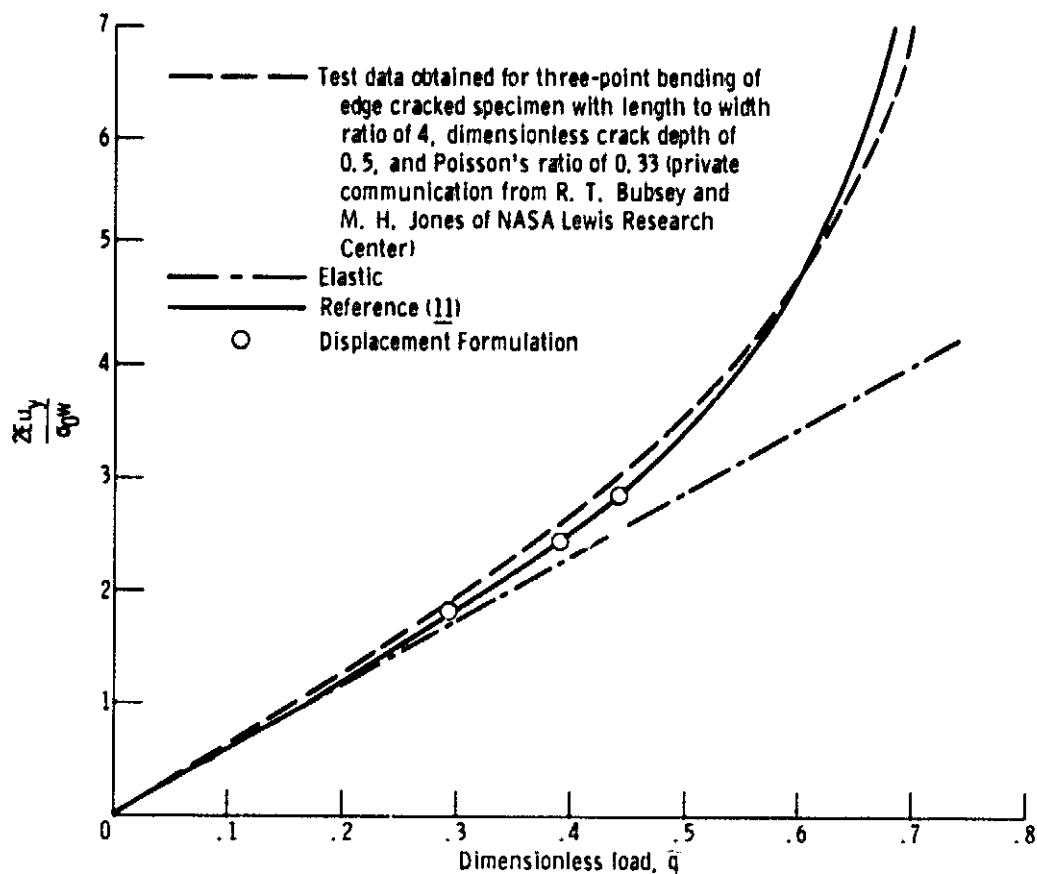


Figure 17. - Dimensionless plane strain y-directional notch opening displacement for specimen with single edge notch subjected to pure bending. Dimensionless notch depth $\bar{a} = 0.5$; notch angle $\alpha = 10^\circ$; Poisson's ratio $\mu = 0.33$; stress-strain curve given by figure 16.

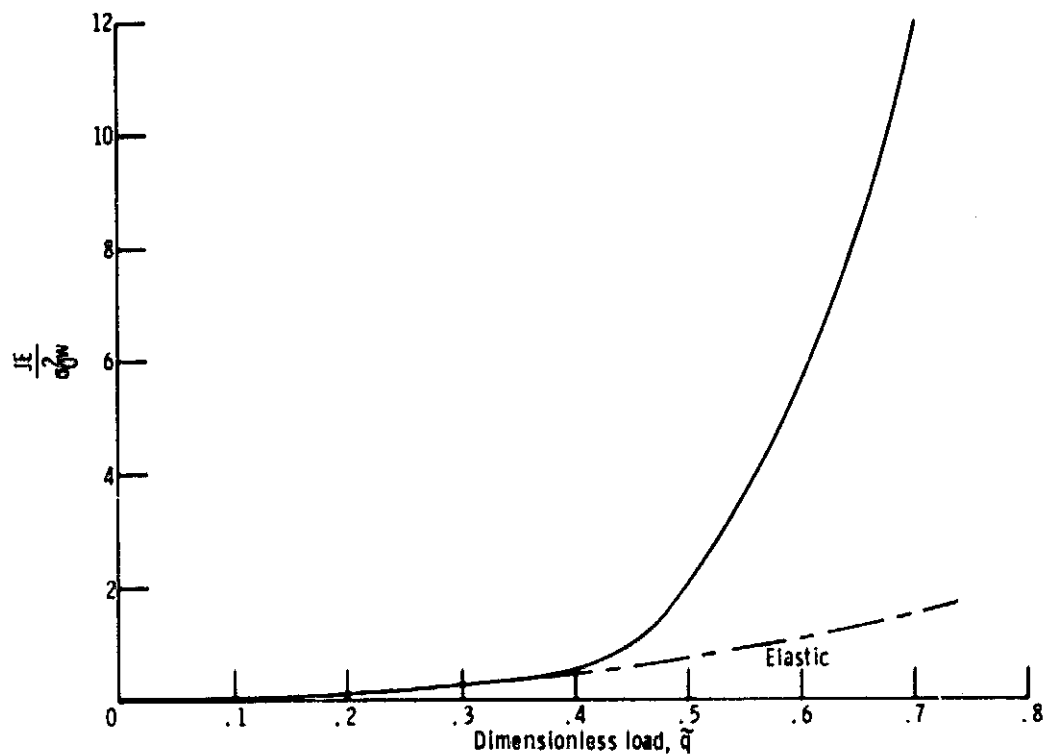


Figure 18. - Dimensionless plane strain J integral for specimen with single edge notch subjected to pure bending. Dimensionless notch depth $\bar{a} = 0.5$; notch angle $\alpha = 10^\circ$; strain hardening parameter $m = 0.05$; Poisson's ratio $\mu = 0.33$.

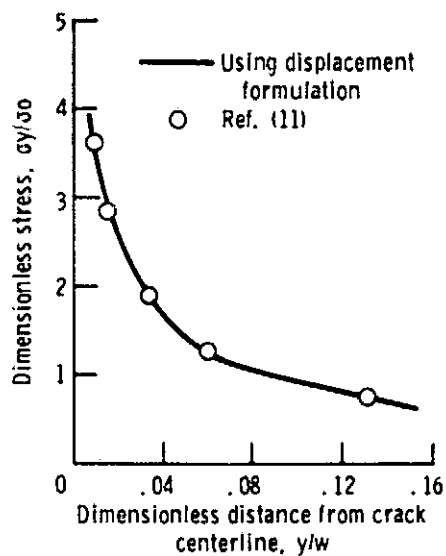


Figure 19. - Dimensionless y-directional stress at a function of distance from notch centerline, $\bar{x} = 0.0074$, $\bar{a} = 0.5$, $\bar{q} = 0.4$.

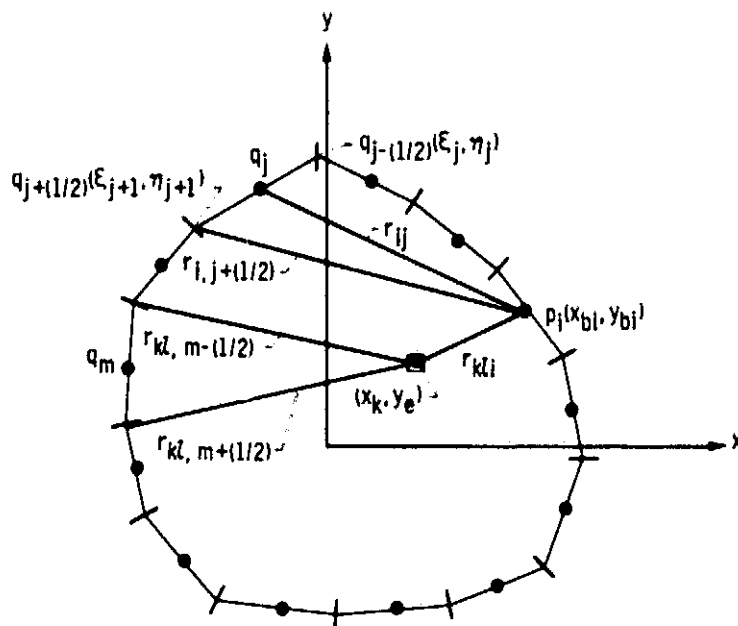


Figure 20. - Boundary and interior notation for computing coefficients given in Appendix A.